PCCP
Physical Chemistry Chemical Physics

This article can be cited before page numbers have been issued, to do this please use: M. Mehring, A. M. Preda, S. Scholz, M. Krasowska, K. Bhattacharyya, A. M. Toma, C. Silvestru, M. Korb, T. Rueffer, H. Lang and A. A. Auer, *Phys. Chem. Chem. Phys.*, 2020, DOI: 10.1039/C9CP06924K.

View Article Online
DOI: 10.1039/C9CP06924K

Evaluation of bismuth-based dispersion energy donors – synthesis, structure and theoretical study of 2-biphenylbismuth(III) derivatives

Ana-Maria Fritzsche,[a,f] Sebastian Scholz,[a] Małgorzata Krasowska,[b] Kalishankar Bhattacharyya,[b] Ana Maria Toma,[a,c] Cristian Silvestru,[c] Marcus Korb,[d,e] Tobias Rüffer,[d] Heinrich Lang,[d,f] Alexander A. Auer,*[b] Michael Mehring*[a,f]

[a]Technische Universität Chemnitz, Fakultät für Naturwissenschaften, Institut für Chemie, Professur Koordinationschemie, 09107 Chemnitz, Germany

[b]Max-Planck-Institut für Kohlenforschung, Kaiser-Wilhelm-Platz 1, 45470 Mülheim an der Ruhr, Germany

[c]Babeş-Bolyai University, Faculty of Chemistry and Chemical Engineering, Department of Chemistry, Supramolecular Organic and Organometallic Chemistry Centre (SOOMCC), 11 Arany Janos, 400028 Cluj-Napoca, Romania

[d]Technische Universität Chemnitz, Fakultät für Naturwissenschaften, Institut für Chemie, Professur Anorganische Chemie, 09107 Chemnitz, Germany

[e]The University of Western Australia, Faculty of Science, School of Molecular Sciences, Crawley, Perth, WA 6009, Australia

[f]Center for Materials, Architectures and Integration of Nanomembranes (MAIN), Rosenbergstr. 6, 09126 Chemnitz

Email: Michael Mehring*- michael.mehring@chemie.tu-chemnitz.de

Email: Alexander Auer* - alexander.auer@kofo.mpg.de

* Corresponding authors

View Article Online
DOI: 10.1039/C9CP06924K

Abstract

A series of 2-biphenyl bismuth(III) compounds of the type $(2\text{-PhC}_6H_4)_{3\text{-}n}BiX_n$ [n = 0 (**1**); n = 1, X = Cl (**2**), Br (**3**), I (**4**), Me (**5**); n = 2, X = Cl (**6**), Br (**7**), I (**8**)] has been synthesized and analyzed with focus on intramolecular London dispersion interactions. The library of the compounds was set up in order to investigate the Bi···π arene interaction by systematic variation of X. The structural analysis in the solid state revealed that the triarylbismuth(III) compound **1** shows an encapsulation of the metal atom but the distances between the bismuth atom and the phenyl centroids amount to values close to or larger than 4.0 Å, which is considered to be a rather week dispersion interaction. In the case of monomeric diorganobismuth(III) compounds **2−5** the moderate crowding effectively hinders the formation of intermolecular donor-acceptor interactions, but allows for intramolecular dispersion-type interactions with the 2-biphenyl ligand. In contrast, the structures of the monoorganobismuth compounds **6−8** show the formation of Bi−X···Bi donor-acceptor bonds leading to the formation of 1D ribbons in the solid state. These coordination bonds are accompanied by intermolecular dispersion interactions with $Bi\cdots Ph_{centroid}$ distances < 4.0 Å. In solution the diorganobismuth(III) halides **2−4** show a broadening of their NMR signals (*H-8,H-8’* and *H-9, H-9’* protons of the 2-biphenyl ligand), which is a result of dynamic processes including ligand rotation. For further elucidation of these processes compounds **2**, **4** and **7** were studied by temperature-dependent NMR spectroscopy. Electronic structure calculations at the density functional theory and DLPNO-Coupled Cluster level of theory were applied to investigate and quantify the intramolecular London dispersion interactions, in an attempt to distinguish between basic intramolecular interactions and packing effects and to shed light on the dynamic behavior in solution.

Keywords: bismuth; 2-biphenyl; London dispersion interaction; single crystal X-ray structure; DFT-D; DLPNO-CCSD(T); electronic structure calculations.

View Article Online
DOI: 10.1039/C9CP06924K

Introduction

Over the past several years, London dispersion interaction of main group elements has witnessed increasing interest both experimentally[1-9] and theoretically,[10-16] and was demonstrated to be relevant in the field of organometallic chemistry with regard to structure and properties even of small molecules. In recent reports it is discussed that weak dispersion interactions of the type metal···π arene contribute significantly to the assembling processes of molecular units in supramolecular structures, which might open up new directions of dynamic structural evolution of supramolecular architectures.[6-8] With regard to this and to build up a better understanding of the basic principles intermolecular London dispersion interactions for diverse arylbismuth compounds have been studied in our research groups,[16-22] and the effect on polymorphism and phase transition in compounds of the type Ar_3Bi (Ar = C_4H_3NMe, C_4H_3O, C_4H_3S, C_4H_3Se) was demonstrated.[18, 21] In the last years, the importance of intramolecular Bi···π arene interactions for the stabilisation of unusual organobismuth compounds, mainly bearing ligands of the terphenyl type, has been demonstrated by several other research groups (Scheme 1).[23-32] Although it is now well accepted that dispersion interaction plays an important role in structure formation, there is still need for systematic investigations in order to determine the influence of *e.g.* the substituents X in organobismuth(III) compounds of the type $Ar_{3-n}BiX_n$ (n = 0, 1, 2). A future aim is to make use of this type of interactions in supramolecular design strategies controlled by the strength and nature of the interaction of aryl ligands with bismuth and other heavy metals.

View Article Online
DOI: 10.1039/C9CP06924K

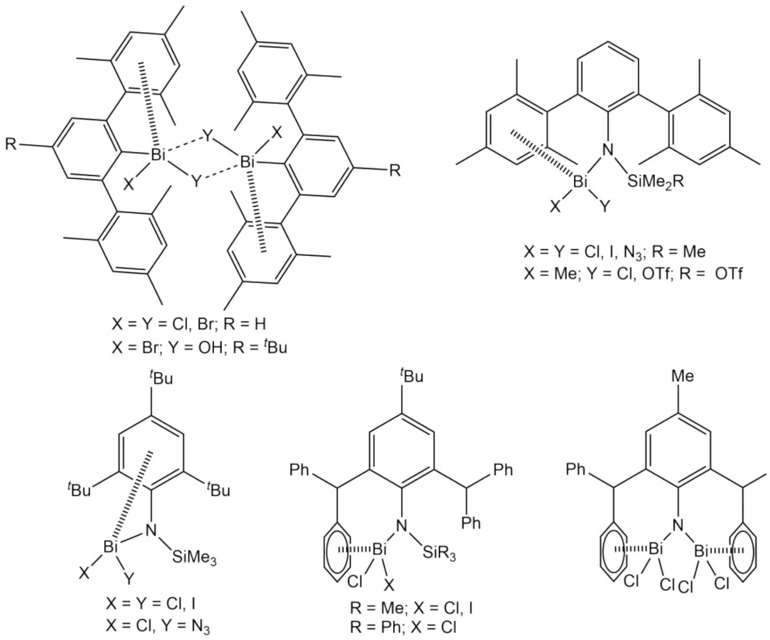

Scheme 1. Selected molecules showing intramolecular Bi$\cdots\pi$ arene interactions with significant impact on structure and reactivity.[24, 27-32]

To reach this goal theoretical work is necessary in addition to experimental studies. So far, computational studies on pnictogen$\cdots\pi$ arene interactions address mainly intermolecular interactions,[13, 16, 20-21, 33] whereas only a limited number of studies on intramolecular interactions of this type is reported.[25, 29, 32] For example, intermolecular pnictogen$\cdots\pi$ arene interaction were investigated earlier using computational methods (BP86-D3/def2-TZVPD level of theory) by Frontera and coworkers on a series of systems involving different types of benzene derivatives and the heavier pnictogenes ECl_3 (E = As, Sb, Bi).[14, 15] In a more recent paper we have investigated the intermolecular interaction between various compounds of the type BiX_3 (X = H, Me, Ph, OH, OMe, F, Cl, Br) and C_6H_6 (Scheme 2, **A**). These studies have shown that the nature and strength of the dispersion interaction is strongly influenced by the substituent X.[16, 20] The higher the bismuth is polarized by X, the stronger is the interaction and the shorter is the Bi$\cdots$Ph$_{centroid}$ distance. The calculations revealed a pure dispersive interaction for the methyl group, while the chlorine substituent induces a significant donor-acceptor behaviour. This interplay between dispersion and donor-acceptor properties results from the ($\pi\rightarrow\sigma^*$) charge transfer. Another study was focused on the As, Sb and Bi adducts $EX_3\cdots C_6H_6$ (X = Me, OMe,

View Article Online
DOI: 10.1039/C9CP06924K

Cl) (Scheme 2, **B**) and it was analysed how the dispersion interaction strength is altered by exchanging the pnictogen E. The interaction energies calculated at the DLPNO-CCSD(T) level increase from As < Sb < Bi and range from -10 kJ mol^{-1} to -40 kJ mol^{-1} for $ECl_3 \cdots C_6H_6$ (E = As, Sb, Bi).[34] In a recent paper we have also discussed the interaction between $BiCl_3$ and benzene derivatives with either one or three substituents being R = CF_3, NO_2, NH_2, OH, OCH(O) (Scheme 2, **C**). The results show that the substituents of the arene have a significant influence on the interaction strength and structure of the formed adducts (e.g. $BiCl_3 \cdots C_6H_5R$) and especially substituents that increase the electron density in the aromatic ring increase the strength of the donor-acceptor interaction and vice versa.[35] The overall interaction energy might transcend -70 kJ mol^{-1} in compounds of the type $BiCl_3 \cdots C_6H_3R_3$.

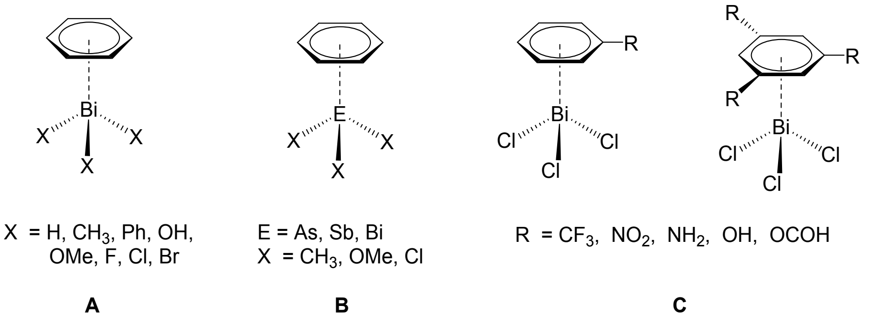

Scheme 2. Different dispersion adducts of aromatic systems with trivalent heavy pnictogen compounds (EX_3).[16, 20, 34, 35]

On the basis of our previous studies here the synthesis, characterization and the crystal structures of the arylbismuth(III) compounds $(2\text{-}PhC_6H_4)_{3-n}BiX_n$ [n = 0 (**1**); n = 1, X = Cl (**2**), Br (**3**), I (**4**), Me (**5**); n = 2, X = Cl (**6**), Br (**7**), I (**8**)] are reported (Scheme 3). They are composed of bismuth acting as DED (Dispersion Energy Donor) and 2-biphenyl as a rigid intramolecular ligand. The influence of the substituent X on the strength of the intramolecular bismuth$\cdots\pi$ arene interaction was analysed experimentally and by using electronic structure calculations.

View Article Online
DOI: 10.1039/C9CP06924K

Results and Discussion

Synthesis

The first report on the synthesis of $(2\text{-}PhC_6H_4)_3Bi$ dates back to 1936, based on the reaction of the Grignard reagent $2\text{-}PhC_6H_4MgBr$ and $BiCl_3$.[36] Later on, the synthesis of the related derivatives of the lighter pnictogens, i.e. $(2\text{-}PhC_6H_4)_3E$ (E = P, As and Sb) using the Wurtz-Fittig method, employing sodium was reported.[37] However, neither the determination of the crystal structures of these compounds nor of their halogen derivatives was published so far.

The compounds reported herein of the type $(2\text{-}PhC_6H_4)_{3\text{-}n}BiX_n$ [n = 0; (**1**); n = 1, X = Cl (**2**), Br (**3**), Me (**5**); n = 2, X = Cl (**6**), Br (**7**)] were prepared either via *i)* salt elimination reactions between 2-biphenyllithium and BiX_3 (X = Cl, Br), (3:1, 2:1 and 1:1 molar ratio), or methyllithium and $(2\text{-}PhC_6H_4)_2BiCl$ in Et_2O solution, at −78 °C (Method A, Scheme 3), or *ii)* solvent-free redistribution reactions between $(2\text{-}PhC_6H_4)_3Bi$ and BiX_3 (1:2 molar ratio) carried out at 130 °C (Method B, Scheme 3). The compounds were isolated as colorless crystalline solids in moderate to good yields. Treatment of the organobismuth(III) bromides in EtOH with KI gave, via halogen exchange reactions (Method C, Scheme 3), the iodides $(2\text{-}PhC_6H_4)_2BiI$ (**4**) and $(2\text{-}PhC_6H_4)BiI_2$ (**8**) as yellow and orange solids in good yields. The compound $(2\text{-}PhC_6H_4)_3Sb$ (**9**) was prepared using the same synthetic procedure as described for **1** and was obtained as a colorless solid (Scheme 3). The compounds **1**−**9** are soluble in common organic solvents, but the bismuth compounds are air and heat sensitive. In solution and in the solid state the compounds slowly decompose and hence should at best be stored under inert conditions. The stability of the organobismuth(III) halides was analysed by time dependent ^1H NMR spectroscopy (see ESI Figures S1 and S2). The compounds decompose in the course of five to six days via redistribution reactions finally leading to the formation of biphenyl.

View Article Online
DOI: 10.1039/C9CP06924K

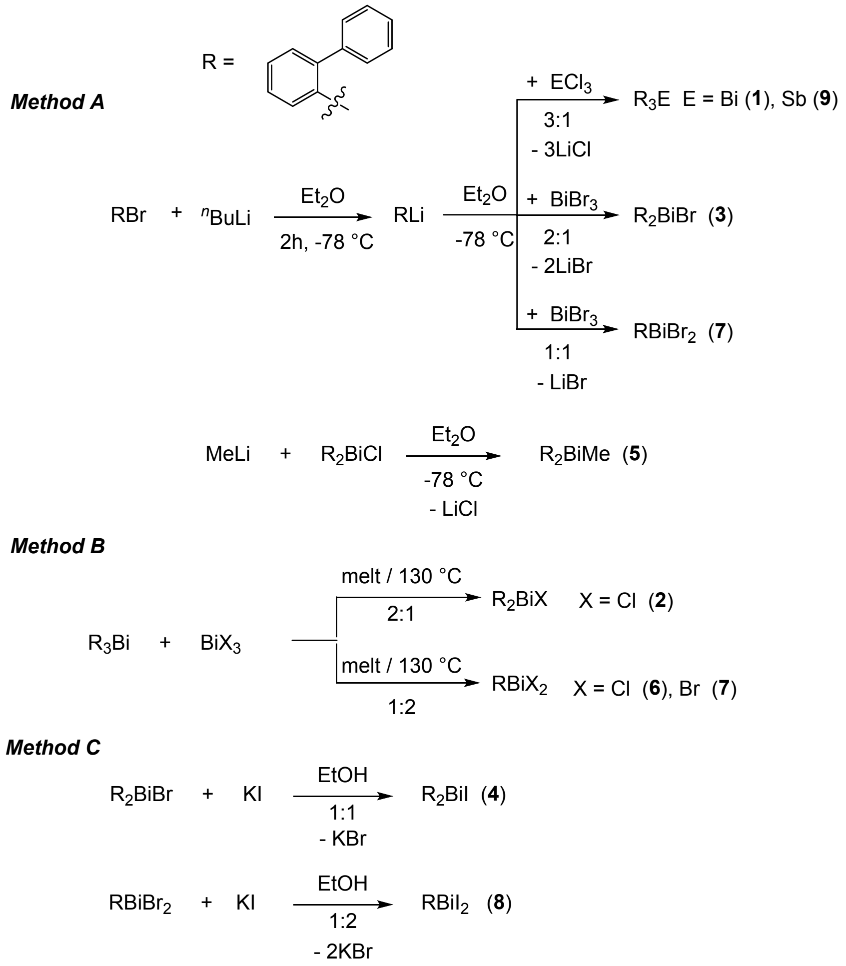

Scheme 3. Synthetic routes for the preparation of the organobismuth(III) compounds (2-$PhC_6H_4)_{3-n}BiX_n$ (**1−8**) and (2-$PhC_6H_4)_3Sb$ (**9**).

*Molecular structures of the triarylpnictogen(III) compounds **1** and **9**.*

Single crystals suitable for X-ray diffraction analysis of **1** were grown from a *n*-hexane solution and the molecular structure is illustrated in Figure 1. Selected bond lengths and angles are listed in the Figure caption and the crystallographic data are given in Table S1. Compound **1** crystallizes in the monoclinic space group $P2_1/n$ and is isomorphous with (2-$PhC_6H_4)_3Sb$ (**9**) (see the ESI, Figure S3). A detailed discussion of the crystal structure of **9** is presented in the ESI. The molecular structure of **1** shows a trigonal pyramidal geometry at the metal atom with average C−E−C bond angles of 94.6° for **1**. The average values of the Bi−C bond lengths of 2.261 Å are within the ranges reported for other arylbismuthine derivatives, *i.e.* Ph_3Bi, [20,38,39] Mes_3Bi[40] and (*p*-tolyl)$_3$Bi.[41]

View Article Online
DOI: 10.1039/C9CP06924K

Compound **1** shows an encapsulation of the bismuth atom by the 2-biphenyl ligands (Bi···Ph$_{centroid}$: 3.99 Å, 4.04 Å and 4.06 Å), however, the Bi···Ph$_{centroid}$ distances are found close to 4.0 Å, which can be considered as the limit of significant London dispersion interaction for these systems based on previous theoretical work.[35] However, the structure of **1** revealed 1D ribbon-like structures (Figure S4i) which are formed via C−H···Ph$_{centroid}$ intermolecular contacts with a distance of C24−H24···Ph$_{centroid}$ 2.55 Å and an angle γ = 5.6° between the ring normal and the vector between the ring centroid and the hydrogen atom. The 1D ribbons are further connected via the C−H···Ph intermolecular contacts C43−H43···Ph$_{centroid}$ 3.06 Å (γ = 10.3°) to give a 2D network in the solid state (see the ESI, Figure S4ii).

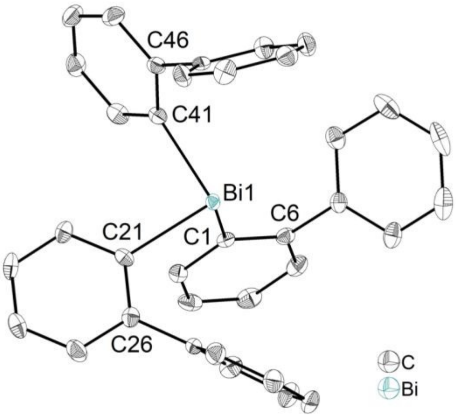

Figure 1. Thermal ellipsoid model of (2-PhC$_6$H$_4$)$_3$Bi (**1**) at 50% probability level. Hydrogen atoms are omitted for clarity. Selected bond lengths [Å]: Bi1−C1 2.258(3), Bi1−C21 2.267(3), Bi1−C41 2.257(4), Bi1···Ph$_{centroid(I)}$ 4.06, Bi1···Ph$_{centroid(II)}$ 4.04, Bi1···Ph$_{centroid(III)}$ 3.99. Selected bond angles [°]: C1−Bi1−C21 95.28(12), C1−Bi1−C41 96.04(12), C21−Bi1−C41 92.33(12), Bi1−C1−C6 118.1(2), Bi1−C21−C26 118.0(3), Bi1−C41−C46 117.0(2).

*Molecular structures of the diarylbismuth halides **2−4** and the diarylmethylbismuthine **5***

Single crystals suitable for X-ray crystallography were isolated upon crystallization at ambient temperature from a *n*-hexane solution (for **2**, **3**), from a CHCl$_3$ solution (for **4**) and by slow diffusion of Et$_2$O into *n*-pentane solution at −28 °C (for **5**). The molecular structures of the diarylbismuth(III) halides are depicted in Figures **2−5**, the selected bond lengths and angles are listed in the Figure captions, and their crystallographic data are given in Table S1. The

View Article Online
DOI: 10.1039/C9CP06924K

compounds crystallize in the triclinic space group *P-1* (**2** and **4**) and the monoclinic space groups $P2_1$/n (**3**) and $P2_1$ (**5**). The asymmetric unit of **2** comprises two crystallographically independent molecules, denoted as 2a (Bi1) and 2b (Bi2). Related bond length and angles of 2a and 2b differ by up to 2%, however, in the following we focus on data of 2a. All the compounds show monomeric structures in the solid state with intramolecular dispersion interactions of the type Bi⋯π arene. The corresponding Bi⋯$\mathrm{Ph_{centroid}}$ distances are Bi1⋯$\mathrm{Ph_{centroid(I)}}$ 3.92 Å (**2a**, Figure 2i), Bi1⋯$\mathrm{Ph_{centroid(I)}}$ 3.82 Å (**3**, Figure 3i) and for **4** Bi1⋯$\mathrm{Ph_{centroid(I)}}$ 3.89 Å and Bi1⋯$\mathrm{Ph_{centroid(II)}}$ 3.98 Å (Figure 4i). The angle γ', which is defined as the angle between the ring normal and the vector between the ring centroid and the bismuth atom, amounts to 46.5°. At least one of the Bi−C−C angles for **2a** (Bi1−C13−C18 116.3(2)°), **3** (Bi1−C13−C18 114.6(3)°) and **4** (Bi1−C1−C6 116.2(8)°, Bi1−C13−C18 117.4()°) is slightly compressed in comparison to the triorganobismuthine **1**. This is indicative for a dispersion interaction between bismuth and one phenyl moiety in **2**−**4**.

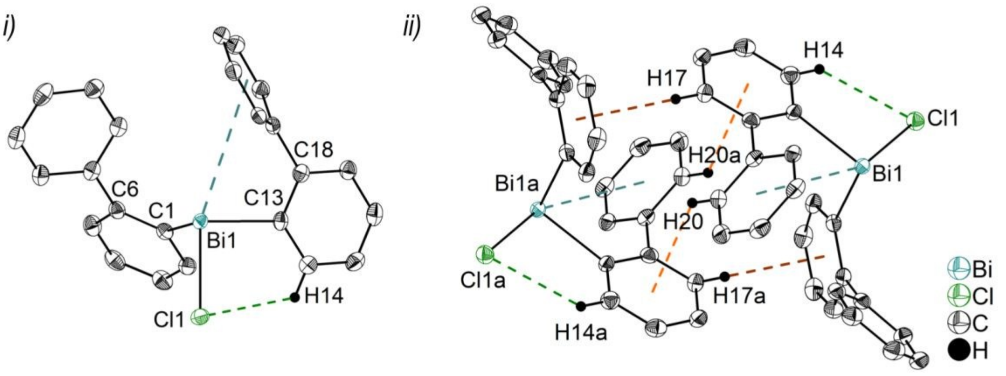

Figure 2. Thermal ellipsoid model of (2-$\mathrm{PhC_6H_4}$)$_2$BiCl (**2**) at 50% probability level showing: *i)* the molecular structure of **2a**. Hydrogen atoms are omitted for clarity, except those involved showing intra- or intermolecular contacts. Selected bond lengths [Å]: Bi1−C1 2.264(3), Bi1−C13 2.263(3), Bi1−Cl1 2.519(1), Bi1⋯$\mathrm{Ph_{centroid(I)}}$ 3.92 (*γ*' = 46.5°), Bi1⋯$\mathrm{Ph_{centroid(II)}}$ 4.26, H14⋯Cl1 2.81. Selected bond angles [°]: C1−Bi1−C13 93.30(12), C1−Bi1−Cl1 89.64(8), C13−Bi1−Cl1 92.89(9), Bi1−C1−C6 120.8(2), Bi1−C13−C18 116.2(2). *ii)* dimer association: C17−H17⋯$\mathrm{Ph_{centroid}}$ 2.73 Å (*γ* = 2.9°), C20−H20⋯$\mathrm{Ph_{centroid}}$ 2.93 Å (*γ* = 6.8°). Symmetry transformations: *a* = 1 − *x*, −*y*, 1 −*z*.

View Article Online
DOI: 10.1039/C9CP06924K

Due to the Bi···π arene interactions the geometry at the bismuth atoms is best described as distorted *pseudo*−trigonal bipyramidal with the $Ph_{centroid}$ *trans* to the halogen atom [$Ph_{centroid}$−Bi1−Cl1 161.9° (for **2**), $Ph_{centroid}$−Bi1−Br1 161.5° (for **3**)] and the carbon atoms placed in the equatorial positions [C1−Bi1−C13 93.30(12)°, C1−Bi1−Cl1 89.64(8)°, C13−Bi1−Cl1 92.89(9)° (for **2a**), C1−Bi1−C13 96.09(17)°, C1−Bi1−Br1 92.33(14)°, C13−Bi1−Br1 93.63(14)° (for **3**)].

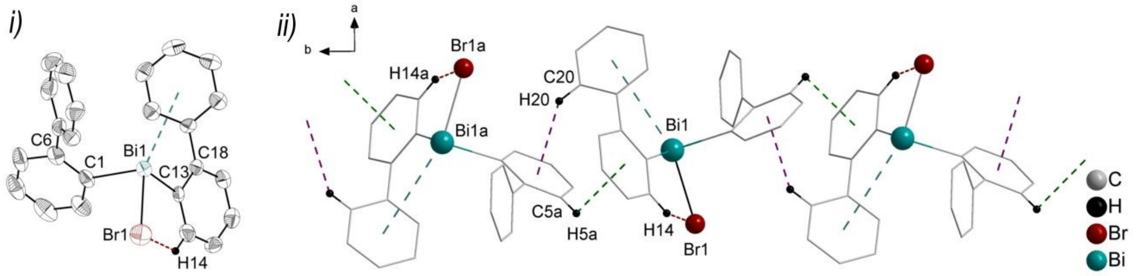

Figure 3. *i)* Thermal ellipsoid model of $(2\text{-}PhC_6H_4)_2BiBr$ (**3**) at 60% probability level. Hydrogen atoms are omitted for clarity, except those involved showing intra- or intermolecular contacts. Selected bond lengths [Å]: Bi1−C1 2.240(5), Bi1−C13 2.252(5), Bi1−Br1 2.655(7), Bi1···$Ph_{centroid(I)}$ 3.82 (γ' = 43.4°), Bi1···$Ph_{centroid(II)}$ 4.06, H14···Br1 2.94. Selected bond angles [°]: C1−Bi1−C13 96.09(17), C1−Bi1−Br1 92.33(14), C13−Bi1−Br1 93.63(14), Bi1−C1−C6 118.8(3), Bi1−C13−C18 114.6(3). *ii)* wire and stick model of 1D ribbons (view along the *c*-axis): C20−H20···$Ph_{centroid}$ 2.94 Å (γ = 12.6°), C5a−$H5a_{arene}$···$Ph_{centroid}$ 3.07 Å (γ = 14.5°). Symmetry transformations: *a* = −1 + *x*, 1 + *y*, *z*.

Intramolecular Bi···Ph contacts in **4** lead to a distorted square pyramidal coordination geometry at the bismuth atom, with the carbon atom C13 of one 2-biphenyl ligand placed in the axial positions. The basal plane of the square pyramid is described by the two $Ph_{centroid}$ ligands, the iodide atom and the carbon atom C1 of the second aryl ligand. This is supported by the bond angles C1−Bi1−C13 of 94.9(4)°, C13−Bi1−I1 of 93.9(3)°, C13−Bi1−$Ph_{centroid(I)}$ of 72.9°, C13−Bi1−$Ph_{centroid(II)}$ of 69.2°, $Ph_{centroid(I)}$−Bi1−I1 of 158.8° and $Ph_{centroid(II)}$−Bi1−C1 of 158.6°.

View Article Online
DOI: 10.1039/C9CP06924K

Compounds **2a** and **4** both form centrosymmetric dimers via two different C−H···Ph intermolecular contacts for **2a** (C17b−H17b$_{\text{arene}}$···Ph$_{\text{centroid}}$ 2.73 Å (γ = 2.9°), C20b−H20b$_{\text{arene}}$···Ph$_{\text{centroid}}$ 2.93 Å, γ = 6.8°, Figure 2ii) and for **4** (C22−H22$_{\text{arene}}$···Ph$_{\text{centroid}}$ 2.77 Å, γ = 6.7°, see Figure 4ii). Moreover, the dimers in **2a** are connected via two additional intermolecular Cl···H contacts, Cl2a···H5c 2.75 Å and Cl1b···H21e 2.86 Å, which results in the formation of a 2D network in the solid state (Figure S5). In **4** the dimeric associates are connected via C−H···Ph$_{\text{centroid}}$ intermolecular contacts with C10−H10$_{\text{arene}}$···Ph$_{\text{centroid}}$ distances of 2.81 Å (γ = 10.7°) leading to the formation of 1D ribbon-like structures (view along the *a*-axis, Figure S6). Noteworthy, compound **3** also forms a 1D ribbon (view along the *c*-axis) in the solid state via two different C−H···Ph$_{\text{centroid}}$ intermolecular contacts with C20−H20···Ph$_{\text{centroid}}$ 2.94 Å (γ = 12.6°), C5a−H5a···Ph$_{\text{centroid}}$ 3.07 Å (γ = 14.5°) (Figure 3ii).

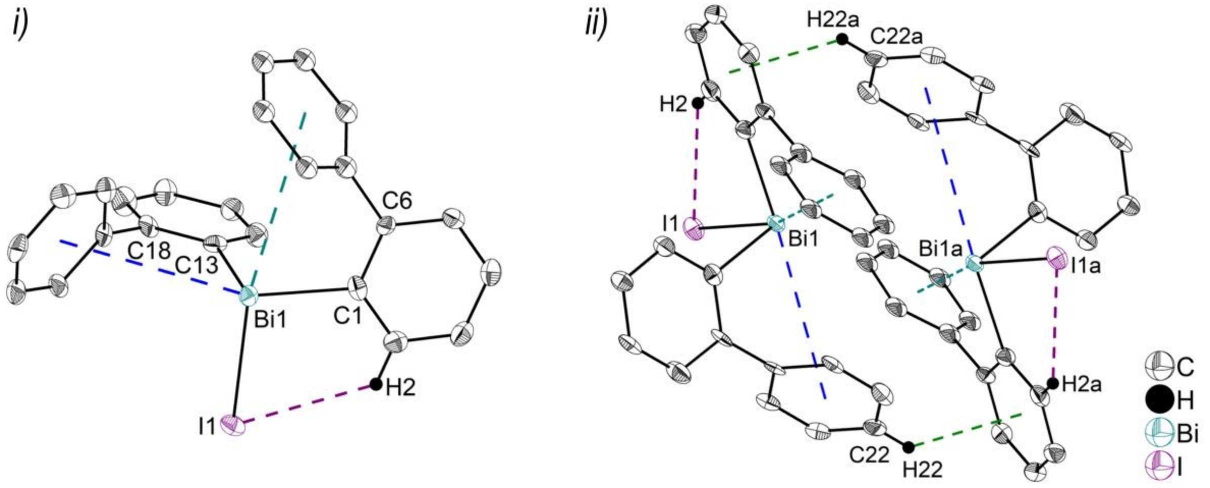

Figure 4. Thermal ellipsoid model of (2-PhC$_6$H$_4$)$_2$BiI (**4**) at 50% probability level showing: *i)* the molecular structure of **4**. Hydrogen atoms are omitted for clarity, except those involved showing intra- or intermolecular contacts. Selected bond lengths [Å]: Bi1−C1 2.264(11), Bi1−C13 2.248(11), Bi1−I1 2.8829(8), Bi1···Ph$_{\text{centroid(I)}}$ 3.89 (γ' = 48.5°), Bi1···Ph$_{\text{centroid(II)}}$ 3.98 (γ' = 39.9°), C2−H2···I1 3.05. Selected bond angles [°]: C1−Bi1−C13 94.9(4), C1−Bi1−I1 94.7(3), C13−Bi1−I1 93.9(3), Bi1−C1−C6 116.2(8), Bi1−C13−C18 117.4(8). *ii)* dimer association: C22−H22···Ph$_{\text{centroid}}$ 2.77 Å (γ = 6.7°). Symmetry transformations: *a* = 1 − *x*, 1 − *y*, 1 – *z*.

View Article Online
DOI: 10.1039/C9CP06924K

In addition the molecules of the monohalides **2a**−**4** reveal the presence of intramolecular C−H···halogen contacts, with distances of C14−H14···Cl1 2.81 Å (for **2a**, Figure 2ii), C14−H14···Br1 2.94 Å (for **3**, Figure 3i) and C2−H2···I1 3.05 Å (for **4**, Figure 4i), which are shorter than the sum of the van der Waals radii of the corresponding atoms (Σr_{vdW} (H, Cl) = 3.02 Å, Σr_{vdW} (H, Br) = 3.06 Å and Σr_{vdW} (H, I) = 3.24 Å).[42] Due to these intramolecular C−X···H interactions, the molecules are arranged in such a way that the halogen atom is placed closer to a 2-biphenyl ligand of the same molecular unit than to the bismuth atom of the neighbouring molecule.

The heteroleptic triorganobismuth(III) compound **5** crystallises in the space group $P2_1$ with two crystallographically independent molecules. Both molecules adopt a distorted trigonal pyramidal geometry at the bismuth atom with average C−Bi−C bond angles of 93.0° (**5a** and **5b**). In **5a** the Bi···Ph$_{\mathrm{centroid}}$ distances are 4.11 Å and 4.19 Å, and 4.10 Å and 4.24 Å in **5b**. The Bi−C−C angles are close to 120° [**5a**: Bi1−C14−C19 120.8(12)° and Bi1−C2−C7 121.0(12)°; **5a**: Bi2−C44−C49 122.5(12)° and Bi1−C32−C37 120.1(13)°;], and thus not indicative for a significant intramolecular interaction between bismuth and the phenyl groups. Intermolecular Bi···Ph$_{\mathrm{centroid}}$ contacts are neither found (Figure S7).

View Article Online
DOI: 10.1039/C9CP06924K

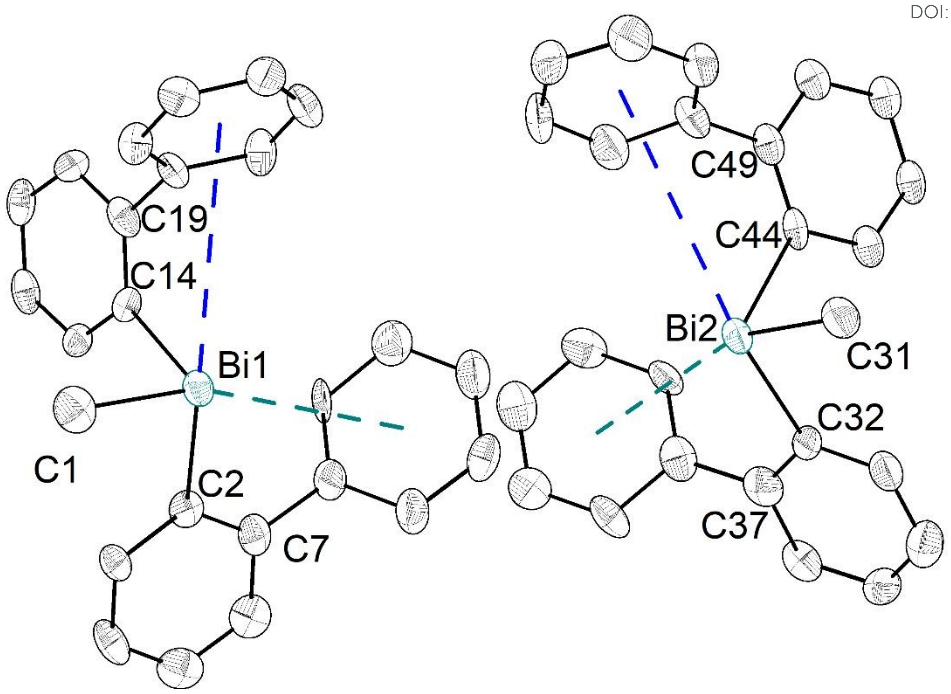

Figure 5. Thermal ellipsoid model of (2-PhC_6H_4)$_2$BiMe (**5**) at 30% probability level. Hydrogen atoms are omitted for clarity. Selected bond lengths [Å]: **5a** (left): Bi1−C1 2.25(2), Bi1−C2 2.263(18), Bi1−C14 2.249(14), Bi1⋯$\mathrm{Ph_{centroid(I)}}$ 4.11 and Bi1⋯$\mathrm{Ph_{centroid(II)}}$ 4.19. Selected bond angles [°]: C1−Bi1−C2 95.0(7), C1−Bi1−C14 89.7(6), C2−Bi1−C14 94.4(6), Bi1−C2−C7 120.8(12), Bi1−C14−C19 121.0(12). **5b** (right): Bi2−C31 2.23(2), Bi2−C32 2.285(17), Bi2−C44 2.265(16), Bi2⋯$\mathrm{Ph_{centroid(I)}}$ 4.10 and Bi2⋯$\mathrm{Ph_{centroid(II)}}$ 4.24. Selected bond angles [°]: C31−Bi2−C32 95.6(7), C31−Bi2−C44 88.9(6), C32−Bi2−C44 94.5(6), Bi2−C32−C37 120.1(13), Bi2−C44−C49 122.5(12).

View Article Online
DOI: 10.1039/C9CP06924K

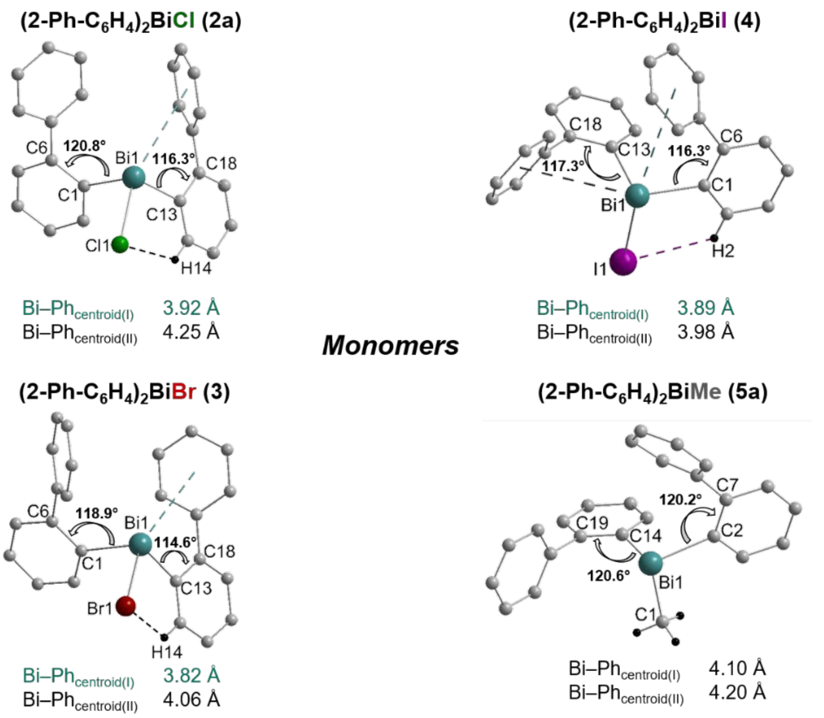

Figure 6. Comparison of the intramolecular Bi···Ph$_{centroid}$ distances and the Bi−C−C bond angles in the monomers of **2a, 3, 4 and5a** as observed in the solid state.

Analysis of the crystal structures of **2−5** reveals that the moderate crowding at the bismuth atom hinders strong intermolecular donor-acceptor interactions and that weak C−H···π arene interactions determine the crystal packing. Intramolecular Bi···Ph contacts are observed in the range 3.82 Å − 4.31 Å for the monomers, with the Bi···Ph$_{centroid}$ distances following the order **3** < **4** < **2** < **5** (Figure 6). It might be concluded, that these interactions hinder free rotation of the biphenyl ligands, but the H···X contacts might also contribute to the stabilization of rotational isomers. For the diorganobismuth halides **2−4**, the Bi−C−C bond angles are significantly compressed (deviation from ideal angle of 120°), while for **5** the Bi−C−C bond angles are close to 120°. This implies that in the organobismuth(III) halides the bismuth···π arene interaction is significantly more attractive in comparison to the triorganobismuth(III) compound **5**. However, the trend for the Bi···Ph$_{centroid}$ distance does not follow the trend predicted for the interaction between bismuth halides and a π arene ligand. This suggests that packing effects in the crystal interfere with the weak intramolecular interaction. In order to assess, quantify and rationalize

DOI: 10.1039/C9CP06924K

these results, an electronic structure calculations on the isolated molecular species was carried out, which will be discussed in a following section.

*Crystal structures of the arylbismuth(III) dihalides **6−8***

Colorless, light yellow and orange single crystals suitable for X-ray crystallography were isolated upon crystallization by slow diffusion of *n*-pentane into Et_2O solution at −28 °C (for **6**), at ambient temperature by slow diffusion of *n*-hexane into $CHCl_3$ solution (for **7**) and from a CH_2Cl_2 solution at ambient temperature (for **8**), respectively. The molecular structures of the arylbismuth(III) dihalides **6−8** are depicted in Figures **7−9**, the selected bond lengths and angles are listed in the Figure captions and their crystallographic data are given in Tables S1 and S2. The compounds crystallize in the orthorhombic space group $P2_12_12_1$ (for **6**), the monoclinic space group $P2_1/c$ (for **7**) and triclinic space group *P-1* (for **8**) respectively. Compound **7** shows a disorder of the 2-biphenyl group with an occupancy ratio of 0.59:0.41. Thus, the supramolecular structures are shown and discussed only for the molecule that shows the higher occupancy for the aryl ring. The asymmetric units of **6** and **7** comprise one molecule of $(2\text{-PhC}_6H_4)BiX_2$, with Bi1–C1, Bi–X1 and Bi–X2 bond lengths of: 2.230(7) Å, 2.684(2) Å and 2.476(2) Å (for **6**); 2.234(11) Å, 3.124(1) Å and 2.610(1) Å (for **7**). Compound **8** shows two crystallographically independent molecules in the asymmetric unit with Bi1−C1, Bi1−I1 and Bi1−I2 bond lengths of 2.247(5) Å, 3.0274(5) Å, 2.8353(5) Å and Bi2−C21, Bi2−I3 and Bi2−I4 bond lengths of 2.257(6) Å, 3.0191(5) Å and 2.8183(5) Å, respectively. The Bi−X bond lengths are in accordance with those observed for primary and secondary Bi-X bonds in other arylbismuth dihalides such as $[PhBiX_2(thf)]$ (X = Cl, Br, I).[43, 44] The crystal structure analyses of **6** and **7** reveal long $Bi\cdots Ph_{centroid}$ distances ($Bi1\cdots Ph_{centroid}$ 3.94 Å for **6**, Figure 7i and $Bi1\cdots Ph_{centroid}$ 3.86 Å for **7**, Figure 8i). For the independent molecules of compound **8** the intramolecular $Bi\cdots Ph_{centroid}$ distances amount to 4.044 Å for molecule **8a** and 3.911 Å for molecule **8b** (Figure 9i). An indication for the intramolecular dispersion type $Bi\cdots\pi$ arene interaction are the Bi1−C1−C6 bond angles (**6**: 117.2(5)°, **7**: 117.1(8)°, **8** 116.7(4) and Bi2−C21−C26 118.3(4)°), which deviate from the ideal angle of 120°. Significant differences were not observed for the intramolecular Bi···Ph$_{centroid}$ distances in **6**−**8**; they are slightly larger than those observed for compounds **2**−**4**. However, a clear trend on the intramolecular Bi···Ph$_{centroid}$ distances related to the nature of X does not become obvious.

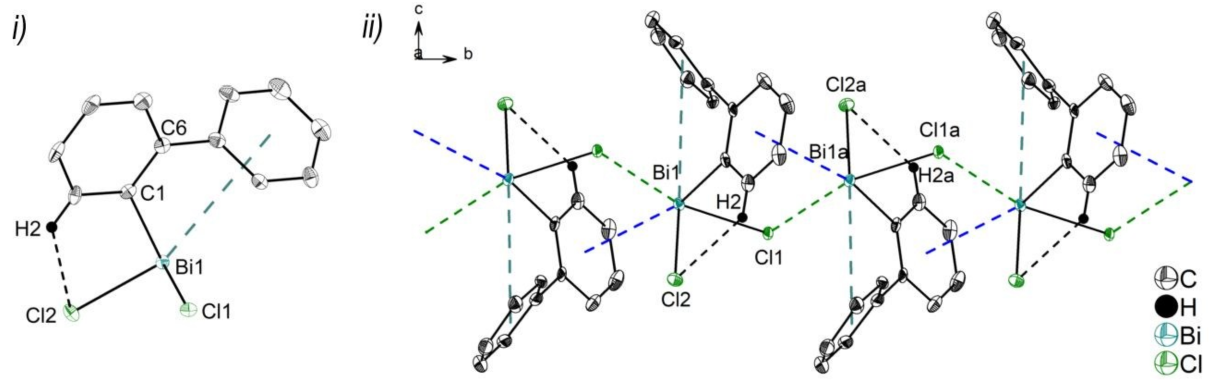

Figure 7. *i)* Thermal ellipsoid model of (2-PhC$_6$H$_4$)BiCl$_2$ (**6**) at 50% probability level and *ii)* 1D ribbon-like structure (view along the *a*-axis). Hydrogen atoms are omitted for clarity, except those involved showing intramolecular contacts. Selected bond lengths [Å]: Bi1−C1 2.230(7), Bi1−Cl1 2.684(2), Bi1−Cl2 2.476(2), Bi1a−Cl1 2.909(2) Å, Bi1···Ph$_{centroid(I)}$ 3.94 (γ' = 50.7°), intermolecular Bi1···Ph$_{centroid(II)}$ 3.42 Å (γ' = 8.9°), C2−H2···Cl2 2.739. Selected bond angles [°]: C1−Bi1−Cl1 85.2(2), C1−Bi1−Cl2 93.6(2), Cl1−Bi1−Cl2 91.8(6), Cl1−Bi1a−Cl1a 165.6(4), Cl1−Bi1a−Cl2a 95.3(6), Bi1−C1−C6 117.2(5), Bi1−Cl1−Bi1a 109.8(1). Symmetry transformations: *a* = 2 − *x*, ½ + *y*, ½ – *z*.

The structures of the arylbismuth(III) dihalides show the formation of 1D ribbons which occurs through short intermolecular Bi···X interactions approximately *trans* to the opposite halogen atom from the neighbouring molecule (**6**: Cl1a−Bi1a···Cl1 165.6(4)°); **7**: Br1a−Bi1a···Br1 167.59(2)°; **8**: I1−Bi1···I3 176.3(14)°; I3a−Bi2a···I1 177.7(14)°). The secondary bridging Bi···X distances are as follows; **6**: Bi1a···Cl1 2.909(2) Å, (cf. Σr_{vdW}(Bi, Cl) 3.82−4.36 Å,[42, 45]); Bi1a···Br1 2.790(1) Å, (cf. Σr_{vdW}(Bi, Br) 3.90−4.40 Å [42, 45]); **8**: Bi1···I3 3.221(5) Å, Bi2a···I1 3.209(2) Å; (Σr_{vdW}(Bi, I) 4.05−4.58 Å [42, 45]). The primary Bi−X distances in the X−Bi···X bridges are, as expected, shorter (**6**: Bi1−Cl1 2.684(2) Å; **7**: Bi1−Br1 3.1240(10) Å; **8**: Bi1−I1 3.027(5) Å, Bi2a−I3a 3.019(5) Å). In addition to these donor-acceptor Bi···X bonds for the dihalides **6**−**8**, intermolecular Bi···π arene interactions between the bismuth atom and the phenyl ring of the neighbouring molecule are established. In combination they lead to the formation of zig-zag chains along the crystallographic axis (1D ribbons in Figures 7ii-9ii). The Bi···$Ph_{centroid}$ distances amount to 3.42 Å (for **6**), 3.70 Å (for **7**), 3.56 Å (for **8**) and are comparable to those observed in [$PhBiX_2$(thf)], (X = Cl, Br, I; Bi···$Ph_{centroid}$ distances in the range between 3.43 Å and 3.54 Å).[43, 44] The competition between donor-acceptor and dispersion interaction is commonly observed for this type of $ArBiX_2$ compounds. The crystal structures **6** and **7** show very similar features, even they are not isostructural. The environment at the bismuth atom for **6** and **7** becomes distorted octahedral based on the core [(2-PhC_6H_4)BiX_3($Ph_{centroid}$)$_2$], with the C1 atom of the biphenyl ligand, the $X_{bridging}$ atoms and the intermolecular $Ph_{centroid}$ occupying the equatorial positions. The $Ph_{centroid}$ involved in intramolecular interaction and the terminal halogen atom are placed in the axial positions with $Ph_{centroid}$−Bi1−Cl2 159.2° (for **6**) and $Ph_{centroid}$−Bi1−Br2 162.3° (for **7**). In **8** the Bi2 atom adopts a distorted square pyramidal geometry with the carbon atom of the biphenyl ligand in apical position and the vector of the intramolecular Bi···$Ph_{centroid}$ contact placed *trans* to the terminal iodide atom I4. This is reflected in the bond angles of $Ph_{centroid}$−Bi2−I4 150.0°, $Ph_{centroid}$−Bi2−C21 69.6°, $Ph_{centroid}$−Bi2−I3 112.4° and C21−Bi2−I3 90.34(17)°. A distorted square pyramidal environment was observed for the Bi1 atom, with the basal plane formed by the carbon atom C1 of the biphenyl ligand, two $I_{bridging}$ atoms and $Ph_{centroid}$, while the axial position is occupied by I2 (cf. corresponding bond angles $Ph_{centroid}$−Bi1−C1 150.2°, I1−Bi1−I3 176.3°, I2−Bi1−C1 96.3°, I2−Bi1−I1 95.1°, I2−Bi3−I1 88.4°, I2−Bi1−$Ph_{centroid}$ 112.4°.

View Article Online
DOI: 10.1039/C9CP06924K

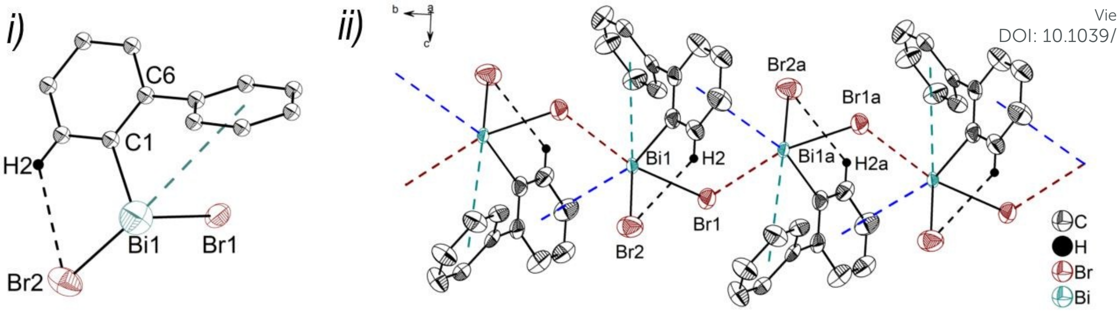

Figure 8. *i*) Thermal ellipsoid model of (2-PhC_6H_4)BiBr_2 (**7**) at 50% probability level and *ii)* 1D ribbon-like structure (view along the *a*-axis). Hydrogen atoms are omitted for clarity, except H2 involved in intramolecular interaction with a bromine atom. Selected bond lengths [Å]: Bi1−C1 2.234(11), Bi1−Br1 3.1240(10), Bi1−Br2 2.6099(13), Bi1−Br1a 2.7911(10), Bi1···$Ph_{centroid(I)}$ 3.86 (γ = 51.1°), intermolecular Bi1···$Ph_{centroid(II)}$ 3.70 Å (γ‘ = 18.0°), C2−H2···Br2 2.991. Selected bond angles [°]: C1−Bi1−Br1 79.9(7), C1−Bi1−Br2 96.9(7), C1−Bi1−Br1a 90.3(7), Br1−Bi1−Br2 95.3(3), Br1−Bi1a−Br1a 167.59(2), Br2−Bi1−Br1a 93.4(3), Bi1−Br1−Bi1a 105.23(3) Bi1−C1−C6 117.1(8), Symmetry transformations: *a* = −*x*, ½ + *y*, ½ – *z*.

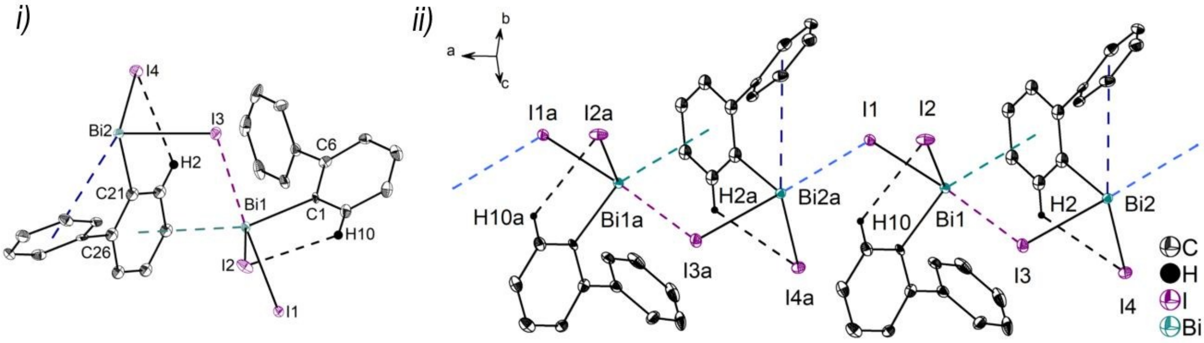

Figure 9. *i)* Thermal ellipsoid model of (2-PhC_6H_4)BiI_2 (**8**) at 50% probability level showing dimer association of molecules **8a** and **8b** and *ii)* 1D ribbon like structure. Hydrogen atoms are omitted for clarity, except H2 and H10 involved in intramolecular interaction with the iodine atoms. Selected bond lengths [Å]: Bi1−C1 2.247(5), Bi1−I1 3.0274(5), Bi1−I2 2.8353(5), Bi2a−I1 3.2091(5) Å, Bi1−I3 3.2205(5) Å, Bi1···$Ph_{centroid(I)}$ 4.04, Bi2−C21 2.257(6), Bi2−I3 3.0191(5), Bi2−I4 2.8183(5), Bi2···$Ph_{centroid(II)}$ 3.91 (γ‘ = 48.7°), intermolecular Bi1···$Ph_{centroid(III)}$, 3.56 Å (γ‘ = 18.9°), C2−H2···I4 3.054, C10−H10···I2 3.054. Selected bond angles [°]:

View Article Online
DOI: 10.1039/C9CP06924K

C1−Bi1−I1 92.88(14), C1−Bi1−I2 96.25(15), C1−Bi1−I3 84.07(14), C21−Bi2−I3 90.34(17), C21−Bi2−I4 94.45(16), C21−Bi2−I1 90.34(14), I1−Bi1−I2 94.078(13), I1−Bi1−I3 176.289(12), I2−Bi1−I3 88.367(13), I3−Bi2−I4 92.031(13), I3a−Bi2a−I1 177.743(12), Bi1−I3−Bi2 98.170(14), Bi1−I1−Bi2a 100.114(14), Bi1−C1−C6 116.7(4), Bi2−C21−C26 118.3(4). *ii)*: Symmetry transformations: *a* = 1 + *x*, *y*, *z*; *b* = − *x*, 1 − *y*, 1 – *z*.

Furthermore, a 2D network is formed based on short intermolecular C−H⋯Cl bonds (for **6**) and C−H_{arene}⋯Ph contacts (for **7** and **8**) between parallel 1D layers connected through C8-H8b⋯Cl2a 2.80 Å (for **6**, Figure S8), C11−H11⋯$Ph_{centroid}$ 2.84 Å (γ = 13.1°, for **7**, Figure S9) and C10−H1A⋯$Ph_{centroid}$ 2.87 Å (γ = 17.1°, for **8**, Figure S10).

*Computational study of diarylbismuth halides **2-4** and the diarylmethlybismuthine **5***

As one of the aims of this study is to rationalize intramolecular Bi⋯π arene interactions using a library of flexible substituents, the crystallographic analyses are supplemented by computational studies. While in most of the presented compounds intermolecular interactions are dominating in the crystal structure, in compounds **2−5** intramolecular Bi⋯π arene interactions seem to dominate. Hence, we start by discussing whether the trends observed in the crystal structures are purely due to intramolecular interactions, or whether crystal packing effects play a major role.

In order to assess the molecular structures of compounds **2-5**, one has to take into account that this particular system has several “soft” degrees of freedom leading to a rich variety of possible conformers. In order to compare and assess the structures found by the crystallographic analysis, first of all, an overview over the most important low energy conformers has to be obtained. For this purpose, a conformational sampling approach recently published by Grimme et al. was carried out.[46] In this scheme, a multistep multilevel procedure is used to screen a large part of the conformational space, select the lowest energy conformers and refine them at a higher level of theory.

View Article Online
DOI: 10.1039/C9CP06924K

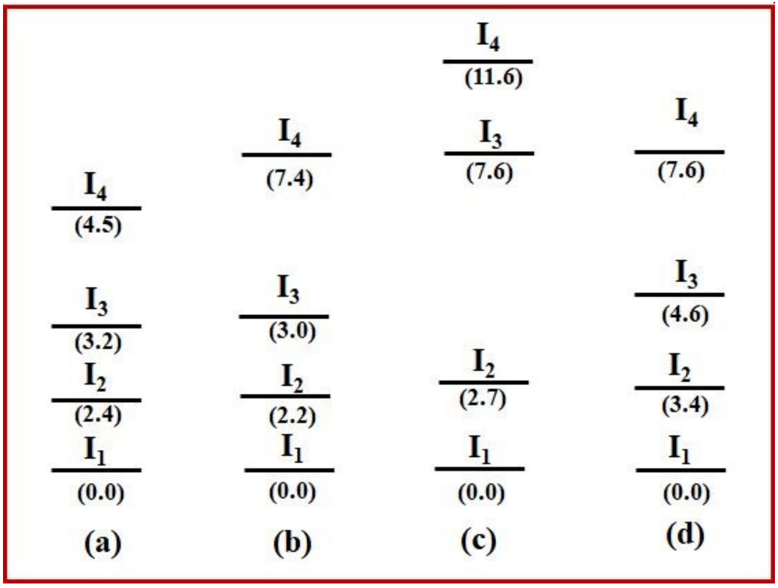

Figure 10. Schematic representation of the four lowest energy conformers **I$_n$** for each compound (a) R_2BiCH_3 (**2**), (b) R_2BiCl (**3**), (c) R_2BiBr (**4**), and (d) R_2BiI (**5**) (R = 2-PhC_6H_4). The lowest energy geometries of each compound are set to zero (energy in kJ/mol, structures see Figs. 11 and 12).

The relative energies of the lowest energy conformations of **2-5** after a final optimization at the PBE-D3/def2-TZVP level of theory are shown in Fig. 10. Note that previous studies have shown that this level of theory provides a good balance between computational effort and accuracy in comparison to high-level methods.[34, 35] The structural parameters, *i.e.* the computed Bi···Ph$_{\text{centroid}}$ distances and the Bi–C–C angle, are displayed in Fig. 11. For all compounds, the same structural motif with one close Bi···Ph contact is found as the lowest energy structure. Given the crystal structures discussed in the previous sections, the results for the fully relaxed structures are quite remarkable. From methyl to iodide, the bismuth-to-phenyl centroid distance and the two Bi–C–C angles with the organic substituents monotonously decrease from 4.11 to 3.76 Å and from 120.6° to 116.0°, respectively, as might be expected for an increasing strength of the intramolecular Bi···π arene interaction.

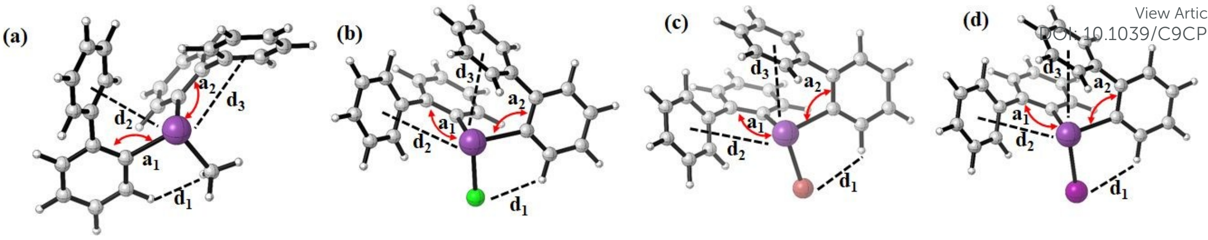

Compound	d$_{1(X\cdots H)}$	d$_{2(Bi\cdots Ph)}$	d$_{3(Bi\cdots Ph)}$	a$_{1(Bi\text{-}C\text{-}C)}$	a$_{2(Bi\text{-}C\text{-}C)}$
(a) R_2BiCH_3 (**2**)	2.68 Å	4.05 Å	4.11 Å	119.4°	120.6°
(b) R_2BiCl (**3**)	2.82 Å	4.05 Å	3.79 Å	119.6°	117.1°
(c) R_2BiBr (**4**)	2.93 Å	4.04 Å	3.77 Å	119.3°	116.5°
(d) R_2BiI (**5**)	3.06 Å	4.04 Å	3.76 Å	119.2°	116.0°

Figure 11. Lowest energy structures of (a) R_2BiCH_3 (**2**), (b) R_2BiCl (**3**), (c) R_2BiBr (**4**), and (d) R_2BiI (**5**) (R = 2-PhC_6H_4) calculated at the PBE-D3/def2-TZVP level of theory. Closest Bi···Ph$_{centroid}$ distances and shortest halide-hydrogen bond lengths are given.

The question is why the structures observed in the crystal do not show the expected trends. Figure 12 includes the structures found in the conformational search and in addition the minimum geometries obtained by optimising the molecular structures as obtained from the single crystal X-ray structure analysis.

View Article Online
DOI: 10.1039/C9CP06924K

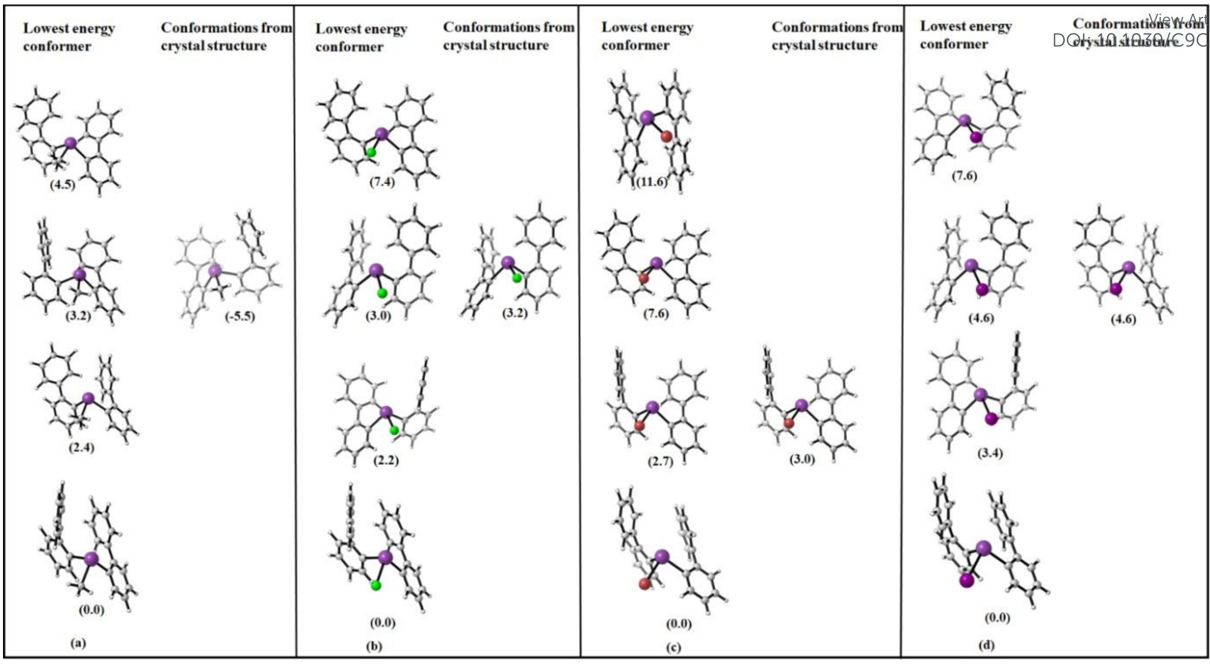

Figure 12. Molecular structures of the four lowest energy conformations of (a) R_2BiCH_3 (**2**), (b) R_2BiCl (**3**), (c) R_2BiBr (**4**), and (d) R_2BiI (**5**) (R = 2-PhC_6H_4) R = (2-PhC_6H_4) (in kJ/mol), and comparison with geometries as obtained by optimization of the molecules geometries in the solid state. Note that the small energy differences between equivalent structures are due to the numerics of the geometry optimizations.

Obviously, none of the conformers found in the crystal structure represents the most stable conformer but the molecular structures derived from **5,** the chloride **3** and iodide **5** resemble each other.

Table 1. Relaxation energies (in kJ/mol) from the experimental crystal structure geometries (with pre-optimized hydrogen atom postions) to the fully optimized conformer (middle column) and comparison to the lowest energy conformer from the GFN-XTB simulation (right column). All structures are optimized at PBE-D3/def2-TZVP level of theory R = (2-PhC_6H_4).

Crystal Structure (experimental)	Optimization at PBE-D3/def2-TZVP level	Comparison with lowest energy conformer
R_2BiCH_3 (**2**)	-60.3	-5.5
R_2BiCl (**3**)	-11.0	-3.2
R_2BiBr (**4**)	-28.1	-3.0
R_2BiI (**5**)	-56.1	-4.6

View Article Online
DOI: 10.1039/C9CP06924K

In Table 1, the energy differences between molecules as present in the crystal (with optimized hydrogen positions) and the fully optimized geometries along with the energy difference to the lowest conformer are given. This energy difference arises at least partially from packing effects but also includes the error of DFT in computing equilibrium geometries. While these two effects might be difficult to disentangle, the size of the observed effect with around 10-70 kJ/mol already allows to estimate that packing effects – especially due to CH···π and π···π interactions in the crystal play a significant role for these structures. This has also been observed in previous work on the crystal structures of arylbismuth(III) compounds in which computational methods have been applied to quantify the effects of intermolecular interactions in crystal structures. Here, it was found that typical Bi···π arene interactions for $BiPh_3$ range in the order of 30-40 kJ/mol while intermolecular CH···π and π···π interactions yield interaction energies of similar strength, which results in a rich polymorphism observed in single crystal X-ray structure analysis.[20]

*Solution NMR studies of compounds **1−9**.*

Compounds **1−9** were investigated by solution ^{1}H and $^{13}C\{^{1}H\}$ NMR spectroscopy at ambient temperature in $CDCl_3$ solution. The assignment of resonance signals is based on 2D NMR (COSY, Figs. S14−S22; HSQC and HMBC) correlation spectra, according to the numbering shown in Scheme 4.

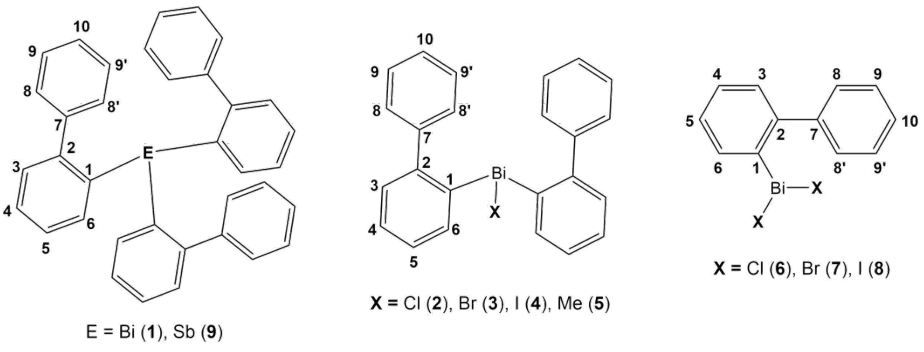

Scheme 4. Compounds **1−9** and numbering scheme for NMR assignments.

View Article Online
DOI: 10.1039/C9CP06924K

The ^{1}H NMR spectra of compounds **1−9** show the expected resonance signals corresponding to the aromatic protons of the 2-biphenyl ligand (Figs. 15 and 16). For the diarylbismuth(III) halides **2−4** and the heteroleptic diaryl(methyl)bismuth(III) compound **5** the ^{1}H NMR spectra show only one set of signals indicating the equivalence of the organic ligands. A very large downfield shift is observed for the resonance signals that belong to the *H-6* proton placed in the *ortho* position to the bismuth atom. The shift depends on the nature of X and increases following the order 2-PhC$_6$H$_4$ < Me < Cl < Br < I (Fig. 13). Characteristic shifts to δ = 8.86 ppm for **2** (X = Cl), 8.96 ppm for **3** (X = Br) and 9.11 ppm for **4** (X = I) are observed, while the triorganobismuth(III) compounds **1** and **5** show resonance signals at δ = 7.91 ppm and δ = 7.97 ppm, respectively. For comparison the corresponding triarylantimony(III) compound **9** was prepared, which shows a resonance signal for the *H-6* proton at δ = 7.37 ppm. Even more pronounced downfield shifts were observed in the case of the monoarylbismuth(III) dihalides **6−8** showing a similar dependence (*vide infra*) on the nature of the substituent X attached to the bismuth atom (Cl < Br < I, Fig. 14). The corresponding resonance signals for *H-6* are observed at δ = 9.78 ppm for **6** (X = Cl), 10.04 ppm for **7** (X = Br) and 10.42 ppm for **8** (X = I). In the literature, a similar trend of the chemical shifts with regard to the halide was described for arylbismuth(III) and arylantimony(III) halides for the signal belonging to the *H-6* proton placed in the *ortho* position to the metal atom. For example, in the series of compounds Ar$_2$EX and ArEX$_2$ (E = Sb, Ar = 2-(Me$_2$NCH$_2$)C$_6$H$_4$, X = Ar, Cl, Br, I),[47, 48] (E = Bi, Ar = 2-(Et$_2$NCH$_2$)C$_6$H$_4$, X = Ar, Cl, Br, I)[49] the chemical shift depends on both the metal atom and on the nature of X, but similar trends with regard to the nature of X are observed (Table 2). There is a small difference between the chemical shifts in compounds of the type Ar$_2$BiX (Δ = 0.10 ppm for Cl < Br and Br < I each, Ar = 2-(Et$_2$NCH$_2$)C$_6$H$_4$),[49] which is in good agreement with the corresponding values for **2−4** (Δ = 0.10 ppm for Cl < Br and Δ = 0.15 ppm for Br < I). In the case of the reported dihalides (Et$_2$NCH$_2$)C$_6$H$_4$)BiX$_2$[49] the differences of the chemical shifts of Δ = 0.14 ppm for Cl < Br and Δ = 0.28 ppm for Br < I are significantly smaller than those found in the compounds **6−8** (Δ = 0.26 ppm for Cl < Br and Δ = 0.38 ppm for Br < I). To the best of

View Article Online
DOI: 10.1039/C9CP06924K

knowledge the chemical shift of δ = 10.42 ppm for *H-6* in (2-PhC_6H_4)BiI_2 is exceptional for arylbismuth(III) halides.

An explanation for the large downfield shift of the hydrogen atom in *ortho* position to the bismuth atom was given by Suzuki and coworkers. Firstly, they point at the participation of *H-6* in hydrogen bonds, *i.e.* the presence of a weak H···halogen interaction, and secondly to the anisotropic deshielding effect due to the proximity of the hydrogen atom to the Bi−X bond as discussed for the chiral bismuthines [2-(Me_2NCH_2)C_6H_4][4-MeC_6H_4]BiX (X = *para*-tolyl, F, Cl, Br, I)[50] and [2-($^tBuSO_2$)C_6H_4][4-MeC_6H_4]BiX (X = Cl, Br).[51] Note that our preliminary calculations of the ^{1}H NMR chemical shifts indicate that the downfield shift is not reproduced using a nonrelativistic approach. It seems likely that the increasing downfield shift is mainly due to the so-called Inverse Halogen Dependence (IHD) which is caused by spin orbit coupling on the heavy halogen atom and its effect on the ^{1}H NMR shift. Similar effects for through space interactions and an IHD have been reported for iodo alkyl and aryl compounds by Kaupp et al. and for ion pairs by Ariai et al.[52, 53]

The ^{13}C{^{1}H} NMR spectra of the di- and monoarylbismuth(III) halides also exhibit a downfield shift for the *C-6* carbon resonance signals, which follows the order Cl < Br < I (**2**: δ = 138.24 ppm, **3**: δ = 139.77 ppm, **4**: δ = 142.75 ppm, Figure S11, **6**: δ = 138.02 ppm, **8**: δ = 140.70 ppm, **9**: δ = 146.35 ppm, Figure S12).

View Article Online
DOI: 10.1039/C9CP06924K

Table 2. ^{1}H NMR chemical shifts and selected distances and angles of compounds **1**−**4** and **6**−**8** and compounds of the general formulas Ar$_2$EX and ArEX$_2$.

Compounds	Substituent X	*Chemical shift* δ (ppm)	H···X distance (Å)	C···X distance (Å)	C−H···X angle (°)	Lit.
Ar$_2$BiX Ar = 2-PhC$_6$H$_4$	Ar (**1**)	7.91	-		-	this work
	Cl (**2**)	8.86	2.808	3.458	126.4	this work
	Br (**3**)	8.96	2.943	3.560	125.1	this work
	I (**4**)	9.11	3.034	3.727	130.9	this work
	Me (**5**)	7.97	-	-	-	this work
Ar$_2$BiX Ar = Ph	Cl	8.30	-	-	-	
	Br	8.36	2.820	3.505	129.0	44
	I	8.41	-	-	-	
Ar$_2$BiX Ar = 2-(Et$_2$NCH$_2$)C$_6$H$_4$	Ar	7.70	-		-	49
	Cl	8.55	2.815	3.436	125.1	49
	Br	8.65	2.925	3.547	125.5	49
	I	8.75	3.128	3.814	132.1	49
Ar$_2$SbX Ar = 2-(Me$_2$NCH$_2$)C$_6$H$_4$	Ar	7.53	-		-	47
	Cl	7.86	2.724	3.360	126.3	48
	Br	7.90	2.838	3.481	125.8	48
	I	7.96	3.104	3.769	129.9	48
ArBiX$_2$ Ar = 2-PhC$_6$H$_4$	Cl (**6**)	9.78	2.739	3.727	130.9	this work
	Br (**7**)	10.04	2.991	3.392	126.5	this work
	I (**8**)	10.42	3.054	3.682	125.1	this work
ArBiX$_2$ Ar = Ph	Cl	8.97	2.732	3.400	129.5	44
	Br	9.12	2.774	3.496	132.6	43
	I	9.22	2.948, 2955	3.677, 3.694	133.0, 135.6	43
ArBiX$_2$ Ar = 2-(Et$_2$NCH$_2$)C$_6$H$_4$	Cl	9.17	-	-	-	49
	Br	9.31	-	-	-	49
	I	9.59	3.077	3.757	129.9	49
ArSbX$_2$[49] Ar = 2-(Me$_2$NCH$_2$)C$_6$H$_4$	Cl	8.28	2.764	3.346	120.4	48
	Br	8.58	2.818	3.473	126.9	48
	I	8.68	3.073	3.738	129.9	48

View Article Online
DOI: 10.1039/C9CP06924K

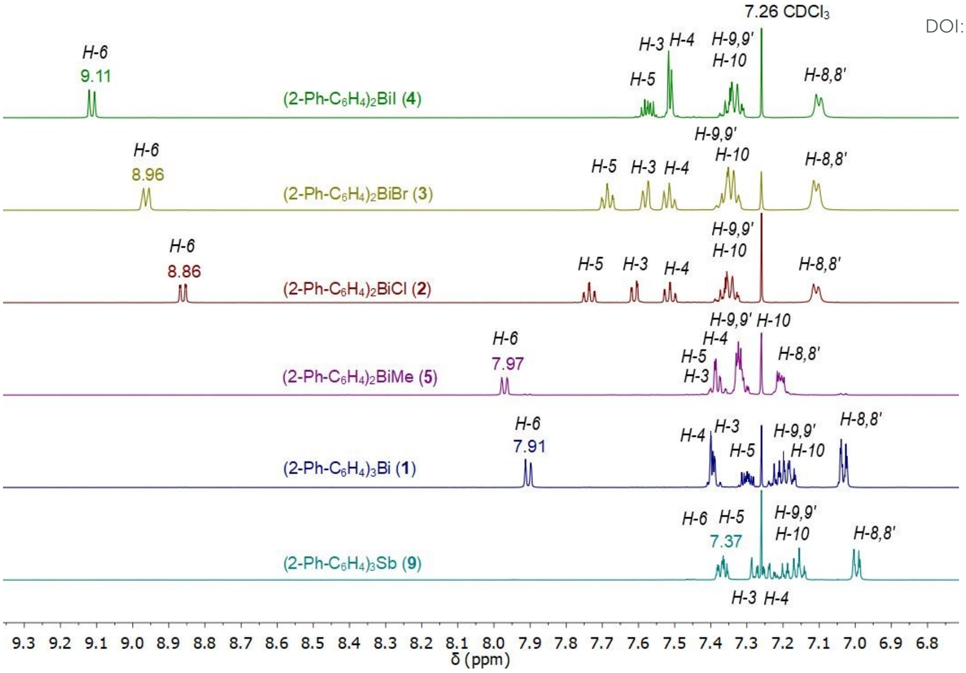

Figure 13. Comparison of ^{1}H NMR spectra (aromatic region) in CDCl$_3$ of compounds **1−5** and **9** showing a large downfield shifts for the resonance signals belonging to *H-6* placed in *ortho* position to the bismuth atom.

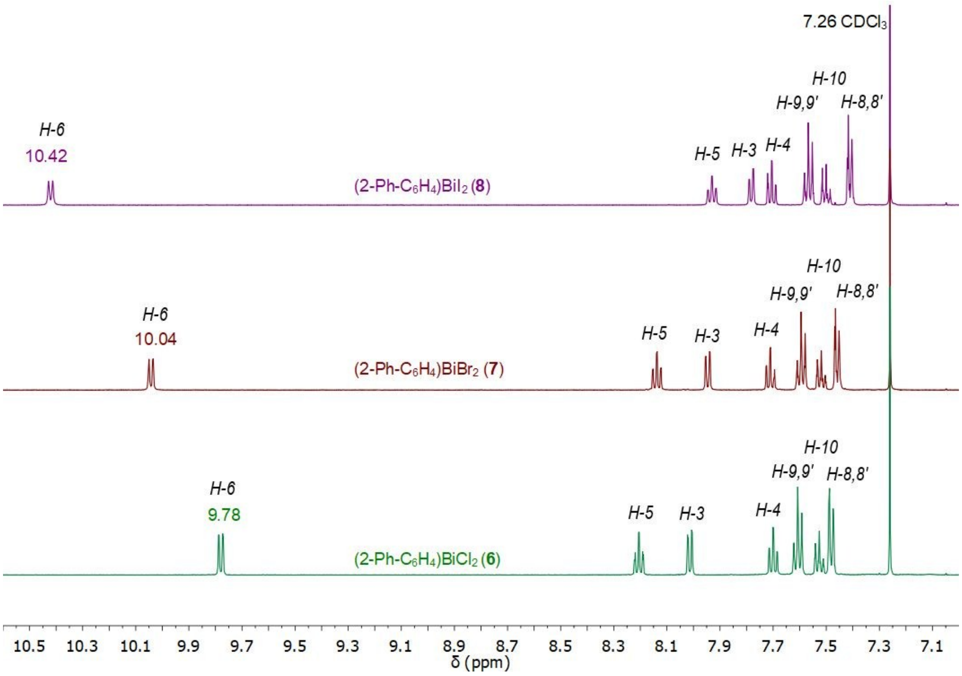

Figure 14. Comparison of ^{1}H NMR spectra (aromatic region) in CDCl$_3$ of compounds **6−8** showing a large downfield shift for the resonance signals belonging to *H-6* placed in *ortho* position to the bismuth atom.

View Article Online
DOI: 10.1039/C9CP06924K

In the ^{1}H NMR spectra of compounds **2−4** significant broadening of the NMR signals at ambient temperature is observed, which is indicative for a dynamic process in solution. In order to study the dynamic behavior, variable temperature ^{1}H NMR spectra were recorded in CD_2Cl_2 for compounds **3** (Figure 15) and **4** (Figure S13), in the temperature range of 293 K to 178 K. At ambient temperature the ^{1}H NMR spectra of **3** and **4** show characteristic resonance signals at $\delta = 7.11$ ppm and $\delta = 7.10$ ppm, respectively, which belong to the *H-8 and H-8'* protons of the biphenyl ligand. This might be interpreted as a result of a dynamic interaction of dispersion type between bismuth and the aryl ligand.

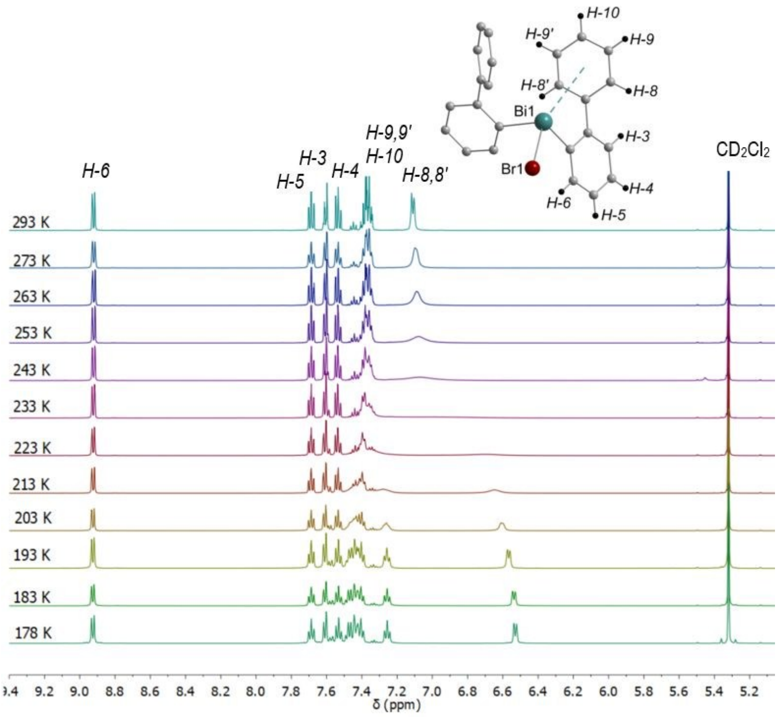

Figure 15. Temperature dependent ^{1}H NMR spectra of $(2\text{-}PhC_6H_4)_2BiBr$ (**3**) measured in CD_2Cl_2 showing the region for aromatic protons including the numbering scheme.

As the temperature was lowered, the resonances belonging to the *H-8 and H-8'* protons further coalesced, with a coalescence temperature (T_c) of 233 K. The corresponding free energies of activation $\Delta G^{\ddagger}$ are 42.8 kJ mol^{-1} for **3** and 43.3 kJ mol^{-1} for **4**. For the signal assigned to the *H-9 and H-9'* protons a broadening is observed above 243 K. By subsequent cooling of the

DOI: 10.1039/C9CP06924K

solution to 178 K, the ^{1}H NMR spectra show two sets of doublet resonances (integral ratio of 1:1), *i.e.* at δ = 6.51 for *H-8* and at δ = 7.47 for *H-8'* in **3**, at δ = 6.66 for *H-8* and δ = 7.44 for *H-8'* in **4** and two sets of triplet resonances (integral ratio of 1:1), *i.e.* at δ = 7.25 for *H-9* and δ = 7.41 for *H-9'* in **3**, and at δ = 7.26 for *H-9* and at δ = 7.39 for *H-9'* in **4**. This assignment is supported by a COSY NMR spectrum of compound **3** at 178 K (Fig. 16). For the aryl protons (*H-3 – H-6*) belonging to the aromatic ring C_6H_4 changes are not observed, being indicative for a fast flip of the aryl ligand. These results indicate that at 293 K the aryl groups attached to the bismuth atom are equivalent and free rotation of the phenyl rings around the C-C bond is allowed, while at low temperature the dynamic process becomes slower, being consistent with the nonequivalence of *H-8* and *H-8'* as well as *H-9* and *H-9'* protons. Thus, in solution the rotation of the phenyl group is frozen, but the Bi···π arene interaction does not freeze. The 2-biphenylbismuth dibromide **7** shows a small upfield shift of its ^{1}H NMR signals (CD_2Cl_2) at 178 K, but no significant changes in comparison to the spectrum measured at 293 K are observed, which indicates the equivalence of *H-8* and *H-8'* as well as *H-9* and *H-9'* in the 2-biphenyl ligand even at low temperature.

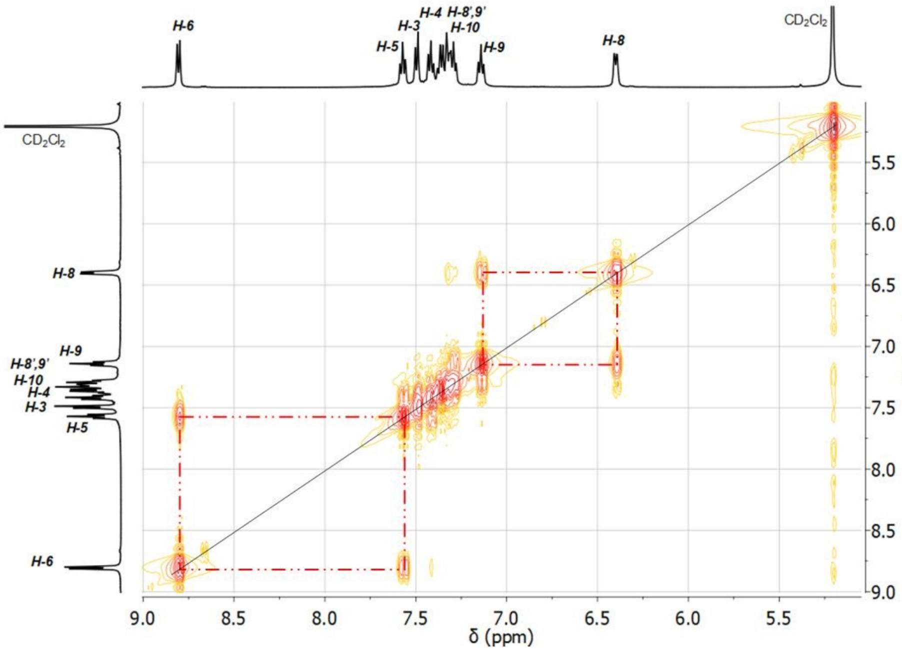

Figure 16. ^{1}H−^{1}H COSY NMR spectrum (500.30 MHz) of $(2\text{-}PhC_6H_4)_2BiBr$ (**3**) recorded in CD_2Cl_2 at 178 K.

View Article Online
DOI: 10.1039/C9CP06924K

Computational Study of the Structural Dynamics

In order to study the internal degrees of freedom that contribute to the structural dynamics in these systems we have first computed potential energy surfaces for the structurally simplest compounds **6−8**, by varying the dihedral angle alpha (see Fig. 17) and beta (see Fig. 18) separately and relaxing all other degrees of freedom at the PBE-D3/def2-TZVP level of theory. The resulting curves are displayed in Figs. 17 and 18 and show that already for only one substituent there are several minima connected by transition states with barriers ranging between a few and 40 kJ/mol.

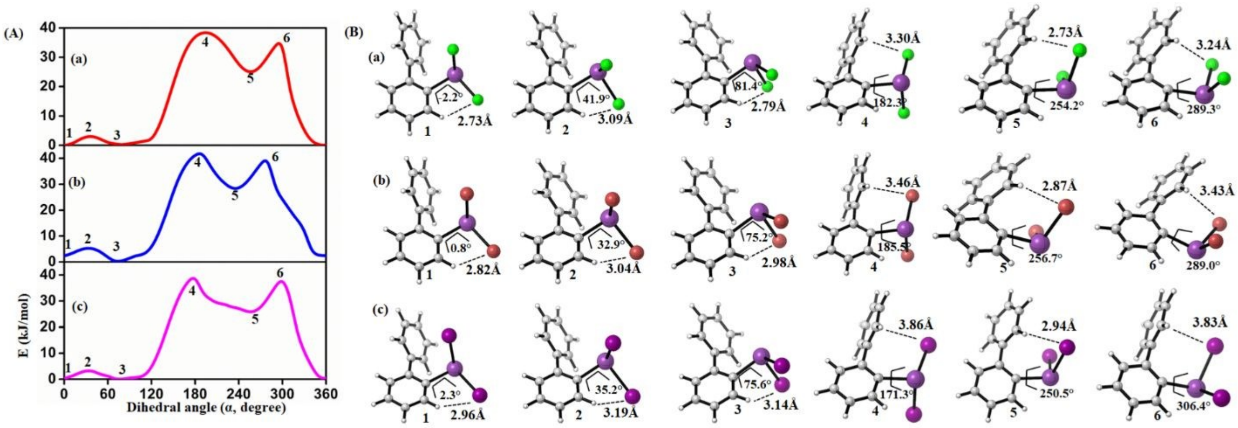

Figure 17. (A) Computed potential energy surfaces (2-PhC$_6$H$_4$)BiX$_2$;(a) X = Cl, (b) X = Br, (c) X = I, along with relaxed C-C-Bi-X dihedral (α) scan at PBE-D3/def2-TZVPP level of theory. (B) Selected conformers of (2-PhC$_6$H$_4$)BiX$_2$ taken from PES; (a) X = Cl, (b) X = Br, (c) X = I. The respective dihedral angle and the shortest hydrogen bond between the nearest hydrogen atom and halogen are shown in each geometry. (1, 3, and 5 (2, 4, and 6) denotes the local minima (maxima) of the respective compound). For details on the dihedral definition see SI.

View Article Online
DOI: 10.1039/C9CP06924K

From the results given in Fig. 17 it is concluded that the BiX_2 moities are able to undergo a pseudo rotation with very low barrier, switching between two hydrogen bonded motifs. A full rotation is hindered by the organic substituent (barrier height of more than 30 kJ/mol) and the halide···π interaction leads to a local minimum high in energy. Note that the barrier for rotation around the central C-C bond in biphenyl itself has been reported as 8-10 kJ/mol. [54]

Table 3: Computed relative energy (in kJ/mol) for the lowest energy conformations of (2-PhC_6H_4)BiX_2 (**6-8**) taken from potential energy surface geometries.

Compound	1	2	3	4	5	6
(2-PhC_6H_4)$BiCl_2$ (**6**)	0.0	3.1	0.2	38.4	24.8	36.4
(2-PhC_6H_4)$BiBr_2$ (**7**)	2.4	5.4	0.0	42.3	28.3	40.7
(2-PhC_6H_4)BiI_2 (**8**)	0.4	3.3	0.0	39.9	25.7	39.03

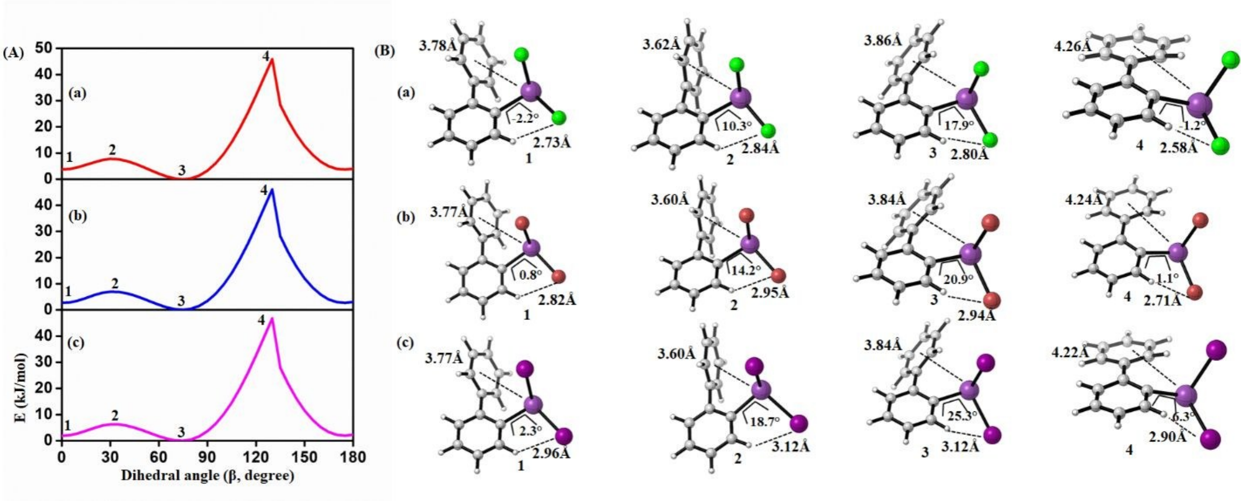

Figure 18. (A) Computed potential energy surface of halogen (X) substituted (2-PhC_6H_4)BiX_2 along with C-C-C-C dihedral (β) rotation at PBE-D3/def2-TZVPP level of theory. (1 and 3 (2 and 4) denotes the local minima (maxima) of the respective compound). (B) Selected conformers of (2-PhC_6H_4)BiX_2 taken from PES; (a) X = Cl, (b) X = Br, (c) X = I. Respective dihedral angle, shortest hydrogen bond distance between the nearest hydrogen(H) atom and halogen(X), center-to-center distance between bismuth atoms and phenyl moieties are shown in each geometry. For details on the dihedral definition see SI.

View Article Online
DOI: 10.1039/C9CP06924K

Fig. 18 depicts the corresponding potential energy surfaces from the rotation of the phenyl moiety which exhibit a low barrier for a 90° tilt connecting two minima with short Bi1···$Ph_{centroid}$ distances. The full rotation, however, is hindered by repulsion of the phenyl ring and the halide substituents as can be concluded from the bond distances and angles as given in Fig. 18 resulting in a barrier of more than 40 kJ/mol.

Table 4: Computed relative energies (in kJ/mol) for the lowest energy conformations of (2-PhC_6H_4)BiX_2 (**6-8**) taken from the potential energy surface.

Compound	1	2	3	4
(2-PhC_6H_4)$BiCl_2$ (**6**)	3.6	7.5	0.0	45.9
(2-PhC_6H_4)$BiBr_2$ (**7**)	2.9	6.9	0.0	46.0
(2-PhC_6H_4)BiI_2 (**8**)	2.1	6.3	0.0	46.7

In order to study and rationalize the effects that we observe for compound **3** in the temperature dependent NMR measurement (see Fig. 15), we have extended the study of the conformational degrees of freedom to include transition states between different conformers. While this system is considerably more complex than that of compounds **6-8**, the minimum structures obtained from the conformational search already indicate which degrees of freedom are decisive for the observed temperature dependence of the NMR in solution.

Starting from the minimum energy conformer (Fig. 12), it can be seen that the protons *H-6* and *H-6'* (see Fig. 15), for example, are not equivalent. However, if compared to its mirror image, the protons *H-6* and *H-6'* are exchanged, while protons *H-8* and *H-8'* are still distinguishable. The barrier that we compute for this process is 22.5 kJ/mol (see Fig. 19), which is well above the estimated conversion barrier for the process observed above 178K. Hence, we conclude that a pseudo-rotation in which the phenyl rings slide across each other converting the structure to its mirror image and averaging the corresponding protons is the process present at low temperatures. This also allows us to assess that the strength of the Bi···π arene

View Article Online
DOI: 10.1039/C9CP06924K

interactions rather falls within this range (below 20 kJ/mol), as the interaction is disrupted and re-established in this process.

Corresponding transition state searches between the different conformers (Fig. 19) exhibit barriers of more than 40 kJ/mol as soon as a full rotation of a phenyl moiety is considered, which is in agreement with the results obtained for the monosubstituted species discussed above. Hence, the averaging of protons *H-8* and *H-8'*, for example, which is observed above 230 K is likely to result from rotation around the central C–C bond in the 2-biphenyl ligand occurring at higher temperatures, for which the major contribution likely comes from steric hindrance during the rotation.

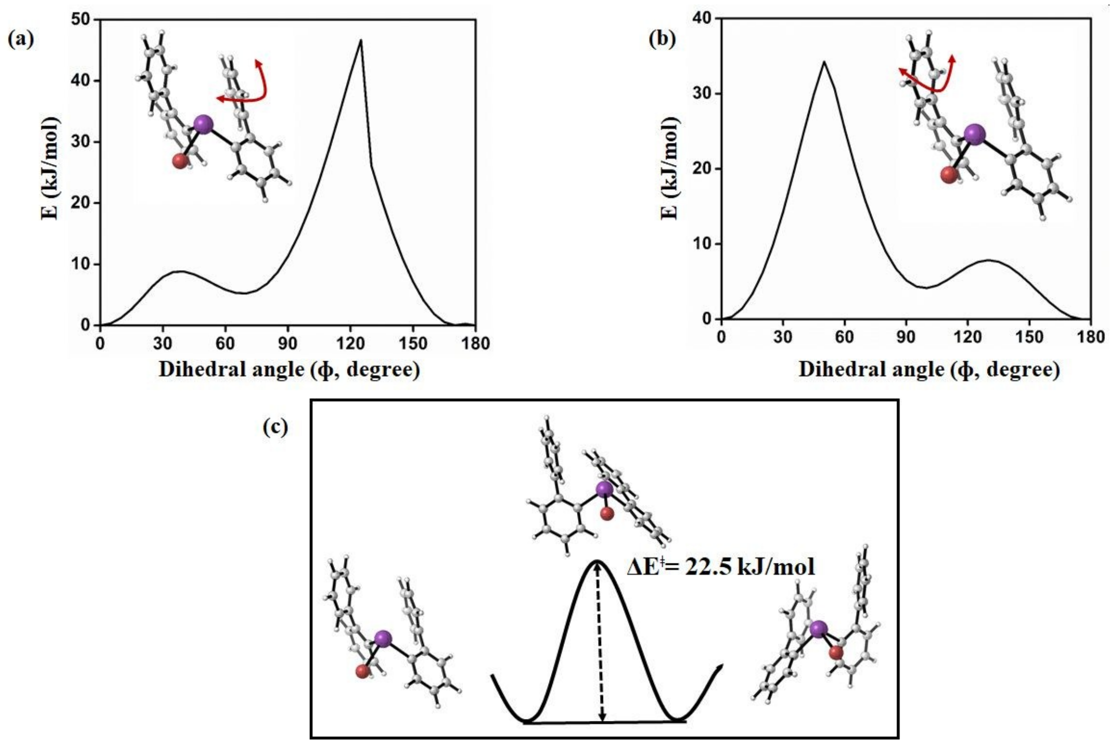

Figure 19. (a), (b) Computed potential energy surface of aryl ring rotation for $(2\text{-}PhC_6H_4)_2BiBr$ (**3**) and (c) Calculated barrier between equivalent conformations of **3**. (PBE-D3/def2-TZVP level of theory.

Thus, we conclude that steric hindrance of the biphenyl ligands rather than a significantly strong dispersion interaction with bismuth is responsible for the trapped rotation of the biphenyl ligand observed in the temperature dependent NMR experiment between 180 K and 220 K.

View Article Online
DOI: 10.1039/C9CP06924K

In order to quantify the Bi···π arene interaction in these compounds in more detail, we have carried out further electronic structure calculations at the DLPNO-CCSD(T) level of theory applying the local energy decomposition (LED) for a molecular model system that allows to express the intermolecular interaction in terms of interactions between molecular fragments (see Fig. 20).

In previous studies it was found that for Bi···π arene interactions a broad range of interaction energies can be observed due to the unique property of heavy main group elements to act as dispersion energy donors and as electron acceptors. For mostly dispersive Bi···π arene interactions as observed in organobismuth compounds, interaction energies around 20 kJ/mol are found, while an additional donor/acceptor component increases the interaction strength to above 40 kJ/mol. In conjuction with aromatic substituents that optimises the donor properties of the arene interaction energies of up to 70 kJ/mol can be obtained.[35] In order to quantify and rationalize the Bi···π arene interaction studied here, we focus on compound **3**. For this purpose, a model structure was constructed that allows to interpret the intermolecular interaction at the DLPNO-CCSD(T) level of theory applying the local energy decomposition (LED). Figure 20 displays the structure and the decomposition of the Bi···π arene interaction strength computed for this model (Table 5).

View Article Online
DOI: 10.1039/C9CP06924K

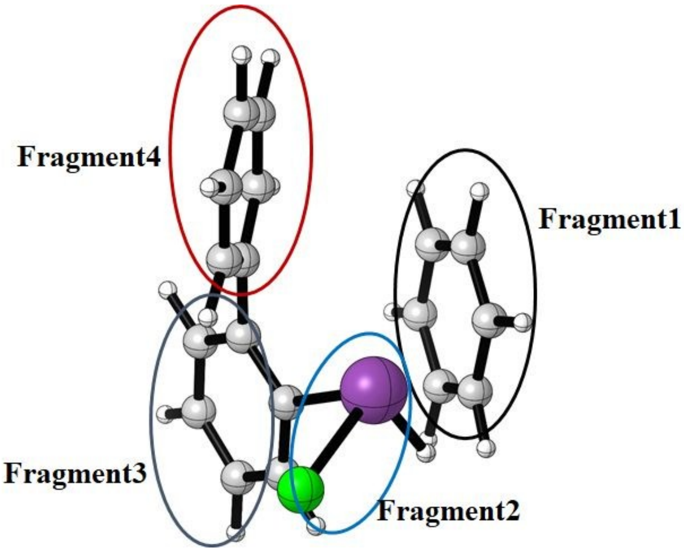

Figure 20. Model system of compound **3** for the study of the Bi···π arene interaction at the DLPNO-CCSD(T) level of theory using the LED scheme. The intramolecular interaction of compound **3** has been converted to an intermolecular interaction by substitution of the biphenyl ligand for H and C_6H_6 (deleting the bismuth bonded phenylene group) while keeping the rest of the structure fixed at the optimized structure of the lowest energy conformer of compound **3**. This allows for a more detailed interpretation of the interactions between the different fragments.

The results clearly indicate that the interaction of the moiety with the shortest Bi···π arene contact is almost exclusively bound by dispersion. A repulsive Hartree-Fock contribution of +43 kJ/mol and a very small attractive non-dispersive correlation contribution (-1 kJ/mol) in the LED which are compensated by the dispersion contribution (-54 kJ/mol) to yield an overall interaction of -21 kJ/mol are typical features of purely dispersive interactions. The Bi···π interaction contributes roughly -23 kJ/mol to the total dispersion interaction in comparison to -21 and -10 kJ/mol for the interaction of this moiety with the biphenyl fragment (see Table 5).

View Article Online
DOI: 10.1039/C9CP06924K

Table 5. Local energy decomposition (LED) analysis and DLPNO-CCSD(T) correlation contributions to total interaction energies (kJ/mol) of the model system of compound **3**. Decomposition of dispersion correlation contribution from fragment are also shown in here.

<table>
<tr><td>$\Delta E_{\text{int}}^{HF}$</td><td>$E_{\text{int}}^{C-CCSD}$</td><td>$\Delta E_{\text{int}}^{C-(T)}$</td></tr>
<tr><td>43.0</td><td>-55.2</td><td>-9.2</td></tr>
<tr><td colspan="3">$\Delta E_{\text{int}}^{total}$ = -21.4</td></tr>
<tr><td>E_{disp}^{C-CCSD}</td><td colspan="2">$\Delta E_{no-disp}^{C-CCSD}$</td></tr>
<tr><td>-54.0</td><td colspan="2">-1.2</td></tr>
<tr><td colspan="3">E_{int}^{C-CCSD} = -55.2</td></tr>
<tr><td>1↔2</td><td>1↔ 3</td><td>1↔ 4</td></tr>
<tr><td>-22.9</td><td>-21.3</td><td>-9.8</td></tr>
<tr><td colspan="3">E_{disp}^{C-CCSD} = -54.0</td></tr>
</table>

At first glance it appears surprising that the nature of the interactions is almost purely dispersive, given the fact that one of the substituents on the bismuth is chlorine, which is known to increase the donor/acceptor character of Bi···π arene interaction. However, the DLPNO-CCSD(T) quantification shows that the interaction strength is in line with what is computed for organobismuth compounds and also falls within the range of the weaker examples for these interactions.

Coming back to the results of the computational study of the barriers associated with the internal degrees of freedom discussed above, the energies in Table 5 also allow to assess, how much of these are caused by the specific Bi···π arene interaction. With an estimate of intramolecular π–π interactions of 20-30 kJ/mol and a Bi···π arene interaction of about 20 kJ/mol it can be argued that while processes which disrupt several of these interactions - like for a rotation of a phenyl moiety (Figs. 19 a and b) – necessarily exhibit barriers in the order of 40 kJ/mol while degrees of freedom in which only the Bi···π interaction is disrupted will exhibit

View Article Online
DOI: 10.1039/C9CP06924K

barriers around 20 kJ/mol. Crystal packing effects, on the other hand, which we estimate to be quite a bit larger than that (around 40 kJ/mol) will in sum dominate structure formation in this case. The analysis of the specific Bi···π arene interaction in these systems is not only in line with the observations from the conformational study and the NMR experiments above, but also explains why crystal packing effects dominate the solid state structures, as CH–π and π–π interactions of the same strength compete with this binding motif.

Discussion and Conclusion

In this work we report on the synthesis and characterisation of a library of compounds of the type $(2\text{-PhC}_6\text{H}_4)_{3\text{-}n}\text{BiX}_n$ [n = 0 (**1**); n = 1, X = Cl (**2**), Br (**3**), I (**4**), Me (**5**); n = 2, X = Cl (**6**), Br (**7**), I (**8**)] and $(2\text{-PhC}_6\text{H}_4)_3\text{Sb}$ (**9**), and study intra- and intermolecular London dispersion interactions. The focus of this work lies on the variation of the intramolecular Bi···π arene interaction strength between the outer phenyl ring of the 2-biphenyl ligand and the bismuth atom upon variation of the ligand X. The triorganobismuth(III) compound **1** shows an encapsulation of the metal atom due to the crowded ligands, but a pronounced dispersion interaction is not observed (bismuth···$\text{Ph}_{\text{centroid}}$ ~4.0 Å). In the less crowded monoarylbismuth compounds $(2\text{-PhC}_6\text{H}_4)\text{BiX}_2$ (**6**−**8**), intramolecular Bi···π arene interactions are present, but the structures are dominated by intermolecular donor-acceptor bonds between the bismuth and halide atoms. Thus, 1D ribbon-like structures are formed. Short intermolecular Bi···$\text{Ph}_{\text{centroid}}$ distances are also observed in these structures, which are shorter than the intramolecular Bi···$\text{Ph}_{\text{centroid}}$ distances and accompany the donor acceptor bonds. The diarylbismuth(III) compounds $(2\text{-PhC}_6\text{H}_4)_2\text{BiX}$ (**2**, X = Cl (**2**), X = Br (**3**), X = I (**4**), X = Me (**5**)) do not show intermolecular donor-acceptor bonds but only intramolecular bismuth···Ph contacts with one of the phenyl groups belonging to the 2-biphenyl ligand. It seems that in this case the moderate crowding leads to the monomeric structures even in the solid state. The single crystal X-ray diffraction analyses of these diorganobismuth(III) compounds revealed that the expectations of shorter Bi···$\text{Ph}_{\text{centroid}}$ distances related to the nature of the halogen substituents and thus to a higher polarizability of the Bi-X moiety is not fulfilled. The shortest distance of 3.82 Å is found

View Article Online
DOI: 10.1039/C9CP06924K

for $(2\text{-PhC}_6H_4)_2BiBr$ (**3**) which is slightly shorter than the longest distance of 3.92 Å as observed for $(2\text{-PhC}_6H_4)_2BiCl$ (**2**), and the corresponding distance of 3.89 Å for $(2\text{-PhC}_6H_4)_2BiI$ (**4**) is found in between. Thus, packing effects, *e.g.* resulting from C−H···Ph contacts have to be considered and make it impossible to draw a meaningful conclusion only from the single crystal X-ray data. A conformational analysis exhibits that the structures found in the experimental crystallographic analysis actually do not correspond to the lowest energy conformers for the isolated molecules. Our results confirm that rather the intermolecular interactions than the intramolecular interactions determine the molecular structure in the solid state. An analysis of the lowest energy structures obtained by conformational search and geometry optimization, on the other hand, show the expected trends for the intramolecular $Bi\cdots Ph_{centroid}$ distances related to the nature of the ligand X in $(2\text{-PhC}_6H_4)_2BiX$. While the acceptor character on the bismuth atom increases (as a result of the interaction with X), the $Bi\cdots Ph_{centroid}$ distance decreases, inducing strain on the substituents which is also reflected in the corresponding Bi–C–C bond angles. In addition to the structural analysis in the solid state NMR spectra in solution were recorded, which reveal information about structural dynamics in solution. A pronounced downfield shift in the ^1H NMR spectra for the resonance signal assigned to the *H*Derived from the experimental observations of the temperature dependence of the NMR chemical shifts, transition state calculations for the different conformers indicate that at high temperatures the phenyl moieties freely rotate. At temperatures below 200 K a process with a barrier of 40 kJ/mol is frozen, lifting the equivalence of several protons, while other pairs of hydrogen atoms, such as the ortho protons, still yield averaged signals. Based on the electronic structure calculations it can be suggested that the low temperature species is the lowest energy conformer, which converts with its mirror image via a process in which the $Bi\cdots\pi$ arene interaction is broken and re-established and which has a barrier in the order of 20 kJ/mol. Hence, the $Bi\cdots\pi$ arene interaction can be estimated to be in the order of 20 kJ/mol or less. This is confirmed by a study of a model compound at the DLPNO-CCSD(T) level of theory applying the local energy decomposition. Thus, the $(2\text{-PhC}_6H_4)_2BiCl$ system, the specific

DOI: 10.1039/C9CP06924K

interaction is suggested to be 23 kJ/mol and the analysis indicates that it is almost purely a dispersion interaction.

Experimental

General procedure

All procedures were carried out under anhydrous nitrogen or argon using standard Schlenk techniques. Solvents were freshly distilled over appropriate drying reagents immediately prior to use. Reagents such as 2-bromobiphenyl were purchased from commercial suppliers and used as received. ATR-FTIR spectra were recorded with a Bio Rad FTS-165 spectrometer (Bio-Rad) with a Golden Gate (SpectroMat) sample adapter. ^{1}H and ^{13}C{^{1}H} NMR spectra were recorded at ambient temperature in $CDCl_3$ (dried over 4 Å molecular sieve) with an *Avance III 500* spectrometer (Bruker) at 500.30 MHz and 125.81 MHz, respectively, and are referenced internally to the deuterated solvent relative to $Si(CH_3)_4$ (δ = 0.00 ppm). NMR signals are given in ppm. The NMR spectra were processed using the software *MestReNova* (version 11.0.4-18998[55]). The temperature dependent ^{1}H NMR spectra were recorded in CD_2Cl_2 at different temperatures from 268 K to 178 K. Calculations of the rate constant k were performed by full line shape analysis with the *DNMR* program, which is implemented in the *TopSpin 2.1* program package. The activation parameters were calculated by use of the *Eyring* equation $k = \frac{RT}{N_A}e^{\frac{-\Delta G^{\neq}}{RT}}$, where R is the general gas constant, T is the absolute temperature, N_A is the *Avogadro* constant, h is the *Planck* constant and $\Delta G^{\neq}$ is the activation *Gibbs* free energy. The CHN-analyses were performed with a *FlashEA 1112* analyzer (Thermo Fisher Scientific). The melting points of compounds were determined with a Melting Point B-540 apparatus (Büchi) and are uncorrected. Powder X-ray diffractograms were measured at ambient temperature with a Stadi P diffractometer (STOE) using Ge(111)-monochromatized Cu-K$_\alpha$ radiation (40 kV, 40 mA). Figures and schemes were created with *ChemDraw Prime*® (version 17.1)[56] and *Origin*® *Pro 2017*. [57]

Crystallographic studies

View Article Online
DOI: 10.1039/C9CP06924K

Crystal data, data collection and refinement parameters for compounds **1−5** and **6−9** are given in Table S1 and Table S2, respectively. Data were collected with either a Rigaku-Oxford Gemini S diffractometer (CrysAlisPro, Version 1.171.38.41l, Rigaku OD, 2015) at 120 K (**1**), 115.7 K (**3**), 100 K (5) and 293 K (**7**) or a Bruker Venture D8 diffractometer (APEX3 v2017.3-0, Bruker AXS) at 100 K (**2**, **4**, **6**, **8** and **9**) using graphite-monochromatized Cu-*Kα* radiation (λ = 1.54184 Å for **1**, **2**, **5**) and Mo-*K*α radiation (λ = 0.71073 Å for **3**, **4**, **6−9**). Crystals of the compounds were embedded in an inert oil (Krytox®, GPL107) and a suitable crystal was selected under an optical microscope and mounted on a CryoLoop (Hampton Research, type: 20 micron and 0.2−0.3 mm diameter), with the CryoLoop fixed on a tiny glass needle. The structures were solved by direct methods using *SHELXS-2013*[58, 59] and refined by full matrix least-squares procedures on F^2 using *SHELXL-2013*.[60, 61] All non-hydrogen atoms were refined anisotropically, while all hydrogen atoms were geometrically placed and refined isotropically in riding modes using default parameters. The crystallographic data for **1−9** have been deposited at the Cambridge Crystallographic Data Centre as supplementary publications CCDC 1948644 (**1**), 1948645 (**2**), 1950689 (**3**), 1948646 (**4**), 1948647 (**5**), 1948648 (**6**), 1950690 (**7**), 1948649 (**8**), 1948650 (**9**) and can be obtained free of charge via https://www.ccdc.cam.ac.uk/. Visualization of the crystal structures was performed with *Diamond* (version 4.5[62]).

PXRD analyses were performed for compounds **1−9** and the diffraction patterns of the measured diffractograms are in good agreement with those simulated from the single crystal X-ray crystallographic data for **1−5**, **7**, **9** (see ESI Figures S23−S27, S29, S31). Only in the case of **6** and **8** a different pattern was observed when comparing to the ones simulated from the single crystal X-ray analyses, most probably due to the formation of polymorphs (see ESI Figures S28, S30). In case of **5** the crystals made available were all observed to be twinned into several different domains, with the major domains comprising about 50% of all reflections. Comparatively high R factor for this kind of structure are assumed to be partial overlap of reflections, while measurements at higher detector distances did not help to get better data.

Computational details

All calculations were performed using the development version of Orca 4.1 program. Initially, we have carried out conformational sampling technique using GFN2-XTB program to get insight in the thermally accessible minimum energy structure of **2-5**. Then, all conformers generated by GFN2-XTB[63, 64] are fully optimized using the PBE[65, 66] density functional in conjunction with the def2-TZVP[67] basis set and the def2/J auxiliary basis set. [68] The default effective core potential[69, 70] (def2-ECP) were used for iodine and bismuth. Fine integration grids (grid 4) were used for DFT optimizations. Stationary points were confirmed by analytical harmonic vibrational frequency calculations. Dispersion correction[71, 72] (D3) with Becke-Johnson (BJ) damping[73] was used for DFT calculations. Based on the relative energy ordering, we have identified the four lowest energy structures for each compound (**2-5**). Transition structure calculation are analysed by frequency calculation to identify only one imaginary frequency at same level of theory. The energies were refined at the DLPNO-CCSD(T) [74-80] level of theory employing the cc-pVQZ[81] basis set for lighter elements (H, C, Cl, and Br). Additionally, the cc-pVQZ-PP[70, 82] and cc-pwCVQZ-PP[83] basis sets combined with the SK-MCDHF-RSC effective core potential were used for iodine and bismuth, accordingly. Additionally, def2/JK,[84] def2/C[85] and cc-pwCVQZ-PP/C[86] (for bismuth) auxiliary basis sets were used in DLPNO-CCSD(T) calculations. TightPNO[87, 88] settings were utilized in all DLPNO-CCSD(T) calculations. Additionally, local energy decomposition[10, 12] (LED) analysis was performed on different conformers of biphenyl compounds in order to analyse dispersion energy contributions in a particular molecule.

Nuclear magnetic shieldings were computed using M06L, [89] TPSS, [90] and double hybrid PBEP86 and utilized pcSseg-3[91] basis set for lighter elements and all-electron Sapporo-DKH3-TZP-2012[92] basis set for bismuth. AutoAux[93] was used to generate auxiliary basis sets for bismuth. Fine integration grids were used (grid 6 for M06L and TPSS, and grid 4 for PBEP86). Resolution of the identity (RI) approximation[94-102] with corresponding auxiliary basis sets were employed in all calculations.

Electronic supplementary information (ESI) available:

View Article Online
DOI: 10.1039/C9CP06924K

Crystallographic data and structure refinement details for **1**−**6** (Table S1) and **7**−**9** (Table S2); ^{1}H NMR spectra of **2** and **7** (Figs. S1 and S2); Single crystal X-ray structures of **9** (Fig. S3) and **1** (Fig. S4); Wire and stick models of supramolecular assemblies of **2** (Fig. S5), **4** (Fig. S6), **5** (Fig. S7) and **6**−**8** (Figs. S8−S10); ^{13}C{^{1}H} NMR spectra of compounds **1**−**5**, **9** (Fig. S11) and **6**−**8** (Fig. S12); temperature dependent ^{1}H NMR spectra of **4** (Fig. S13); ^{1}H−^{1}H COSY NMR spectra of **1**−**9** (Figs. S14−S22); PXRD pattern of compounds **1**−**9** (Fig. S23−S31). CCDC 1948644 (**1**), 1948645 (**2**), 1950689 (**3**), 1948646 (**4**), 1948647 (**5**), 1948648 (**6**), 1950690 (**7**), 1948649 (**8**), 1948650 (**9**).

*Synthesis of (2-PhC$_6$H$_4$)$_3$Bi (**1**)*

A solution of ^{n}BuLi in *n*-hexane (5.5 mL, 2.5 M, 13.75 mmol) was added dropwise at −78 °C to a stirred solution of 2-bromobiphenyl (3.038 g, 13.21 mmol) in anhydrous Et_2O (30 mL). The reaction mixture was stirred for 2 h at −78 °C. After that the organolithium derivative was added dropwise to a solution of $BiCl_3$ (2.036 g, 6.46 mmol) in Et_2O (30 mL), the reaction mixture was kept at −78 °C for 1 h and then stirred overnight at ambient temperature. The solvent was removed in vacuo and the oily residue was extracted with toluene (3 x 15 mL), filtrated off and after removal of the solvent in vacuo, a colorless solid was isolated. Single crystals suitable for X-ray analysis were grown from a *n*-hexane solution. Yield: 2.925 g (68 %). M.p. = 205-206 °C. Elemental analysis calcd. (%) for $C_{36}H_{27}Bi$ (668.58 g·mol^{-1}): C, 64.67; H, 4.07. Found: C, 64.28; H, 4.02. ATR FTIR (cm^{-1}): 3054 (m), 3033 (m), 2364 (m), 2330 (m), 1889 (w), 1856 (w), 1822 (w), 1756 (w), 1598 (w), 1573 (m), 1552 (w), 1452 (s), 1440 (s), 1427 (s), 1382 (w), 1327 (w), 1311 (w), 1282 (w), 1261 (w), 1244 (m), 1178 (m), 1157 (m), 1111 (m), 1072 (m), 1059 (w), 1030 (m), 1013 (w), 995 (w), 980 (m), 965 (w), 946 (m), 914 (m), 876 (w), 843 (m), 770 (s), 747 (vs), 726 (s), 697 (vs), 669 (w), 645 (m), 615 (s), 548 (s), 532 (s), 442 (s), 432 (s), 413 (w). ^{1}H NMR (500.30 MHz, $CDCl_3$): δ 7.03 [m, 6H, *H-8,8'*, C_6H_5), 7.20 [m, 9H, *H-9,9'*, *H-10,* C_6H_5), 7.30 [m, 3H, *H-5*, C_6H_4), 7.39 [m, 6H, *H-3*, *H-4*, C_6H_4), 7.91 (d, 3H, *H-6*, $^3J_{H-H}$ = 7.2 Hz, C_6H_4). ^{13}C{^{1}H} NMR (125.81 MHz, $CDCl_3$): δ 127.16 (s, *C-10*), 127.67 (s, *C-4*), 128.20 (s, *C-*

View Article Online
DOI: 10.1039/C9CP06924K

9,9'), 129.11 (s, *C-8,8'*), 129.62 (s, *C-5*), 130.04 (s, *C-3*), 139.53 (s, *C-6*), 144.96 (s, *C-7*), 149.57 (s, *C-2*), 160.33 (s, *C-1*).

*Synthesis of (2-PhC$_6$H$_4$)$_2$BiCl (**2**)*

A mixture of (2-PhC$_6$H$_4$)$_3$Bi (0.868 g, 1.29 mmol) and BiCl$_3$ (0.205 g, 0.65 mmol) was melted and stirred in the absence of any solvent for 15 minutes at 130 °C. After cooling to ambient temperature, the solid product was extracted with Et$_2$O (300 mL), the solution was filtered and the solvent was evacuated in vacuo to give a colorless solid, followed by extraction with *n*-hexane (500 mL). Single crystals suitable for X-ray analysis were grown from a saturated *n*-hexane solution. Yield: 0.689 g (64 %). M.p. = 132-134 °C. Elemental analysis calcd. (%) for C$_{24}$H$_{18}$BiCl (550.84 g·mol^{-1}): C, 52.33; H, 3.29. Found: C, 52.27; H, 3.25. ATR FTIR (cm^{-1}): 3054 (m), 3036 (m), 3021 (m), 2998 (w), 2346 (w), 1894 (w), 1821 (w), 1574 (w), 1493 (w), 1455 (m), 1443 (s), 1430 (m), 1391 (w), 1285 (w), 1242 (w), 1177 (w), 1158 (w), 1072 (m), 1059 (w), 1026 (w), 1005 (s), 996 (w), 969 (w), 914 (m), 868 (w), 847 (w), 774 (s), 743 (vs), 723 (m), 700 (vs), 646 (w), 632 (m), 550 (s), 525 (m), 436 (s). ^{1}H NMR (500.30 MHz, CDCl$_3$): δ 7.11 (d, 4H, *H-8,8'*, C$_6$H$_5$), 7.35 (m, 6H, *H-9,9', H10,* C$_6$H$_5$), 7.51 (ddd, 2H, *H-4*, $^3J_{\text{H-H}}$ = 7.5 Hz, $^4J_{\text{H-H}}$ = 1.3 Hz, C$_6$H$_4$), 7.61 (dd, 2H, *H-3*, $^3J_{\text{H-H}}$ = 7.6 Hz, $^4J_{\text{H-H}}$ = 1.3 Hz, C$_6$H$_4$), 7.74 (ddd, 2H, *H-5,* $^3J_{\text{H-H}}$ = 7.4 Hz, $^4J_{\text{H-H}}$ = 1.4 Hz, C$_6$H$_4$), 8.86 (dd, 2H, *H-6*, $^3J_{\text{H-H}}$ = 7.6 Hz, $^4J_{\text{H-H}}$ = 1.3 Hz, C$_6$H$_4$). ^{13}C{^{1}H} NMR (125.81 MHz, CDCl$_3$): δ 128.21 (s, *C-10*), 128.46 (s, *C-8,8'*), 128.76 (s, *C-4*), 129.40 (s, *C-9,9'*), 131.46 (s, *C-3*), 132.40 (s, *C-5*), 138.24 (s, *C-6*), 143.59 (s, *C-7*), 148.54 (s, *C-2*), 180.98 (s, *C-1*).

*Synthesis of (2-PhC$_6$H$_4$)$_2$BiBr (**3**)*

A solution of ^{n}BuLi in *n*-hexane (2.25 mL, 2.5 M, 5.62 mmol) was added dropwise at −78 °C to a stirred solution of 2-bromobiphenyl (1.191 g, 5.10 mmol) in anhydrous Et$_2$O (30 mL). The reaction mixture was stirred for 1 h at −78 °C. After the organolithium derivative was added

View Article Online
DOI: 10.1039/C9CP06924K

dropwise to a solution of $BiBr_3$ (1.146 g, 2.55 mmol) in Et_2O (40 mL), the reaction mixture was kept at −78 °C for 2 h and then stirred overnight at ambient temperature. The solvent was evacuated in vacuo and the oily residue was extracted with $CHCl_3$, the solution filtered and after removal of the solvent in vacuo a colorless solid was isolated. Single crystals suitable for X-ray analysis were grown from a *n*-hexane solution. Yield: 0.158 g (10%). M.p. = 149-150 °C. Elemental analysis calcd. (%) for $C_{24}H_{18}BiBr$ (595.28 g·mol^{-1}): C, 48.42; H, 3.05. Found: C, 48.65; H, 3.00. ATR FTIR (cm^{-1}): 3037 (m), 2992 (w), 2951 (w), 2342 (w), 1598 (w), 1572 (m), 1552 (w), 1494 (m), 1448 (m), 1440 (s), 1427 (m), 1307 (w), 1282 (w), 1267(w), 1240 (m), 1178 (w), 1157 (w), 1107 (w), 1074 (m), 1057 (w), 1032 (w), 1003 (s), 994 (m), 983 (w), 970 (w), 945 (w), 916 (m), 874 (w), 845 (m), 769 (s), 745 (vs), 724 (s), 695 (vs), 670 (s), 645 (s), 615 (s), 550 (s), 528 (s), 432 (s). ^{1}H NMR (500.30 MHz, $CDCl_3$): δ 7.11 (d, 4H, *H-8,8’,* C_6H_5), 7.35 (m, 6H, *H-9,9’, H-10*, C_6H_5), 7.51 (ddd, 1H, *H-4*, $^3J_{H\text{-}H}$ = 7.4 Hz, $^4J_{H\text{-}H}$ = 1.4 Hz, C_6H_4), 7.58 (dd, 2H, *H-3*, $^3J_{H\text{-}H}$ = 7.5 Hz, $^4J_{H\text{-}H}$ = 1.6 Hz, C_6H_4), 7.69 (ddd, 1H, *H-5*, $^3J_{H\text{-}H}$ = 7.4 Hz, $^4J_{H\text{-}H}$ = 1.5 Hz, C_6H_4), 8.96 (dd, 1H, *H-6*, $^3J_{H\text{-}H}$ = 7.6 Hz, C_6H_4). $^{13}C\{^1H\}$ NMR (125.81 MHz, $CDCl_3$): δ 128.22 (s, *C-10*), 128.47 (s, *C-8,8’*), 128.73 (s, *C-4*), 129.32 (s, *C-9,9’*), 131.14 (s, *C-3*), 132.59 (s, *C-5*), 139.77 (s, *C-6*), 143.66 (s, *C-7*), 148.49 (s, *C-2*), 175.66 (s, *C-1*).

*Synthesis of (2-PhC$_6$H$_4$)$_2$BiI (**4**)*

Solid KI (0.064 g, 0.38 mmol) was added to a solution of $(2\text{-}PhC_6H_4)_2BiBr$ (0.176 g, 0.29 mmol) in EtOH (20 mL). The color of the solution turned immediately yellow and the reaction mixture was stirred for two days at ambient temperature. After removal of the solvent in vacuo, the yellow powder was extracted with toluene (3 x 5 mL), the solution filtered and the solvent was removed in vacuo to give a yellow powder. Yield: 0.116 g, (61 %). Single crystals suitable for X-ray analysis were grown from a $CHCl_3$ solution. M.p. = 138-139 °C. Elemental analysis calcd. (%) for $C_{24}H_{18}BiI$ (642.28 g·mol^{-1}): C, 44.88; H, 2.82. Found: C, 44.70.; H, 2.93. ATR FTIR (cm^{-1}): 3053 (m), 3019 (m), 2965 (w), 2343 (w), 1574 (m), 1491 (m), 1454 (m), 1441 (s), 1425 (m), 1387 (w), 1333 (w), 1258 (s), 1242 (m), 1179 (m), 1154 (m), 1091 (s), 1071 (s), 1025 (s), 1004 (vs), 966 (m), 942 (w), 913 (m), 867 (m), 842 (m), 796 (s), 772 (s), 742 (vs), 721 (s), 696

View Article Online
DOI: 10.1039/C9CP06924K

(vs), 642 (s), 613 (s), 547 (s), 525 (s), 484 (w), 434 (vs). ^{1}H NMR (500.30 MHz, $CDCl_3$): δ 7.10 (d, 4H, *H-8,8'*, $^3J_{H\text{-}H}$ = 6.5 Hz, C_6H_5), 7.29–7.39 (m, 6H, *H-9,9', H-10*, C_6H_5), 7.51 (m, 4H, *H-3* + *H-4*, C_6H_4), 7.54–7.61 (m, 2H, *H-5*, C_6H_4), 9.11 (d, 3H, *H-6*, $^3J_{H\text{-}H}$ = 7.4 Hz, C_6H_4). $^{13}C\{^1H\}$NMR (125.81 MHz, $CDCl_3$): δ 128.18 (s, *C-10*), 128.39 (s, *C-8,8'*), 128.68 (s, *C-4*), 129.16 (s, *C-9,9'*), 130.47 (s, *C-3*), 132.77 (s, *C-5*), 142.75 (s, *C-6*), 143.87 (s, *C-7*), 148.44 (s, *C-2*), 165.80 (s, *C-1*).

Synthesis of $(2\text{-}PhC_6H_4)_2BiMe$ (***5***)

A solution of MeLi in Et_2O (0.65 mL, 1.6 M, 1.04 mmol) was added dropwise, via syringe to a stirred suspension of $(2\text{-}PhC_6H_4)_2BiCl$ (**3**) (0.511g, 0.93 mmol) in anhydrous Et_2O (80 mL) at − 78 °C. The reaction mixture was kept at −78 °C for 1 h and then stirred overnight at ambient temperature. The solvent was evacuated in vacuo and the light yellow isolated precipitate was extracted with *n*-pentane (3 x 30 mL), the solution was filtered and after removal of the solvent in vacuo a colorless oil was isolated. Colorless single crystals suitable for X-ray analysis were grown from diffusion of Et_2O into a *n*-pentane solution at −28 °C. Yield: 0.310 g (63 %). M.p. = 83-84 °C. Elemental analysis calcd. (%) for $C_{25}H_{21}Bi$ (530.42 g·mol^{-1}): C, 56.61; H, 3.99. Found: C, 56.91; H, 3.85. ATR FTIR (cm^{-1}): 3056 (m), 3025 (m), 2919 (m), 2346 (w), 2284 (w), 1871 (w), 1752 (w), 1599 (w), 1572 (w), 1499 (w), 1455 (w), 1443 (m), 1420 (w), 1389 (w), 1244 (w), 1177 (w), 1153 (w), 1111 (w), 1071 (m), 1030 (w), 1007 (m), 965 (m), 913 (m), 872 (w), 843 (w), 778 (m), 747 (vs), 718 (s), 700 (vs), 666 (w), 642 (w), 552 (m), 523 (m), 450 (s), 438 (s).^{1}H NMR (500.30 MHz, $CDCl_3$): δ 0.97 (s, 3H, CH_3), 7.21 (m, 4H, *H-8,8'*, C_6H_5), 7.32 (m, 8H, *H-9,9', H10*, C_6H_5, *H*-4, C_6H_4), 7.38 (m, 4H, *H-3, H5*, C_6H_4), 7.97 (d, 2H, *H-6*, $^3J_{H\text{-}H}$ = 7.8 Hz, C_6H_4). $^{13}C\{^1H\}$ NMR (125.81 MHz, $CDCl_3$): δ 13.46 (s, CH_3), 127.26 (s, *C-10*), 127.62 (s, *C-4*), 128.33 (s, *C-9,9'*), 129.11 (s, *C-5*), 129.15 (s, *C-8,8'*), 129.41 (s, *C-3*), 138.26 (s, *C-6*), 145.18 (s, *C-7*), 149.50 (s, *C-2*), 151.03 (s, *C-1*).

Synthesis of $(2\text{-}PhC_6H_4)BiCl_2$ (***6***)

View Article Online
DOI: 10.1039/C9CP06924K

A mixture of (2-$PhC_6H_4)_3Bi$ (0.868 g, 1.29 mmol) and $BiCl_3$ (0.205 g, 0.65 mmol) was melted and stirred for 10 minutes at 130 °C, in the absence of any solvent. After cooling to ambient temperature, the solid product was extracted with Et_2O (300 mL), the solution filtered and the solvent was evacuated in vacuo to give a colorless solid, that was washed with *n*-hexane (5 x 10 mL). Finally, the solid material was extracted with CH_2Cl_2 to give a colorless microcrystalline solid. Colorless single crystals suitable for X-ray analysis were grown from diffusion of *n*-pentane into a Et_2O solution at −28 °C. Yield: 0.128 g (30 %). M.p. = 181-183 °C. Elemental analysis calcd. (%) for $C_{12}H_9BiCl_2$ (433.08 g·mol^{-1}): C, 33.28; H, 2.09. Found: C, 31.82; H, 2.09. ATR FTIR (cm^{-1}): 3054 (m), 3017 (w), 2347 (w), 2325 (w), 1983 (w), 1894 (w), 1830 (w), 1574 (w), 1495 (w), 1455 (w), 1443 (s), 1432 (m), 1420 (m), 1075 (w), 1059 (w), 1005 (w), 953 (w), 924 (m), 860 (w), 781 (m), 741 (vs), 722 (s), 704 (vs), 612 (w), 548 (m), 521 (m), 432 (s). ^1H NMR (500.30 MHz, $CDCl_3$): *δ* 7.48 (m, 2H, *H-8,8‘,* C_6H_5), 7.53 (t, 1H, *H-10,* C_6H_5), 7.61 (m, 2H, *H-9,9‘,* C_6H_5), 7.71 (ddd, 1H, *H-4*, $^3J_{H\text{-}H}$ = 7.5 Hz, $^4J_{H\text{-}H}$ = 1.2 Hz, C_6H_4), 8.01 (dd, 1H, *H-3*, $^3J_{H\text{-}H}$ = 7.6 Hz, $^4J_{H\text{-}H}$ = 1.3 Hz, C_6H_4), 8.21 (ddd, 1H, *H-5*, $^3J_{H\text{-}H}$ = 7.5 Hz, $^4J_{H\text{-}H}$ = 1.3 Hz, C_6H_4), 9.78 (dd, 1H, *H-6*, $^3J_{H\text{-}H}$ = 7.8 Hz, $^4J_{H\text{-}H}$ = 1.2 Hz, C_6H_4). $^{13}C\{^1H\}$ NMR (125.81 MHz, $CDCl_3$): *δ* 128.51 (s, *C-8,8‘*), 129.44 (s, *C-10*), 130.04 (s, *C-4*), 130.72 (s, *C-9,9‘*), 133.53 (s, *C-3*), 134.81 (s, *C-5*), 138.02 (s*, C-6*), 141.84 (s, *C-7*), 148.08 (s, C-*2*), *C-1* could not be detected.

*Synthesis of (2-$PhC_6H_4)BiBr_2$ (**7**)*

Method A: A solution of ^{n}BuLi in *n*-hexane (1.72 mL, 2.5 M, 4.29 mmol) was added dropwise at −78 °C via a syringe, to a stirred solution of 2-bromobiphenyl (1.000 g, 4.29 mmol) in anhydrous Et_2O (50 mL). The reaction mixture was stirred for 1 h at −78 °C. After that a solution of $BiBr_3$ (1.925 g, 4.29 mmol) in Et_2O (90 mL) was added, the reaction mixture was kept at −78 °C for 2 h and then stirred for four days at room temperature. The solvent was evacuated in vacuo and the oily residue was extracted with toluene and $CHCl_3$, followed by filtration of the extract and removal of the solvent in vacuo to give an oily light brownish precipitate which was washed with *n*-hexane (5 x 10 mL). Yield: 0.799 g (36%) Yellow single crystals suitable for X-ray analysis were grown from diffusion of *n*-hexane into $CHCl_3$ solution (v/v 1:3).

DOI: 10.1039/C9CP06924K

Method B: A mixture of (2-PhC_6H_4)$_3$Bi (0.796 g, 1.19 mmol) and $BiBr_3$ (1.068 g, 2.38 mmol) was melted and stirred for 15 minutes at 130 °C in the absence of any solvent. After cooling to ambient temperature the solid product was extracted with Et_2O (20 mL), the solution filtered and the solvent was evacuated in vacuo to give 0.280 g (45%) of the title compound as light yellow powder. M.p. = 189-192 °C. Elemental analysis calcd. (%) for $C_{12}H_9BiBr_2$ (521.99 g·mol^{-1}): C, 27.61; H, 1.74. Found: C, 27.39; H, 1.55. ATR FTIR (cm^{-1}): 3058 (w), 3037 (w), 2346 (w), 2136 (w), 1594 (w), 1573 (m), 1548 (w), 1494 (m), 1481 (w), 1452 (s), 1444 (s), 1415 (s), 1344 (w), 1311 (m), 1285 (m), 1269 (m), 1239 (m), 1178 (m), 1157 (s), 1112 (m), 1074 (s), 1053 (s), 1003 (w), 974 (s), 953 (m), 920 (s), 878 (m), 849 (s), 778 (s), 750 (vs), 743 (vs), 719 (s), 706 (vs), 646 (m), 612 (m), 544 (s), 517 (s), 428 (s), 412 (m). ^{1}H NMR (500.30 MHz, $CDCl_3$): δ 7.46 (m, 2H, *H-8,8'*, C_6H_5), 7.53 (t, 1H, *H-10,* $^3J_{H\text{-}H}$ = 7.5 Hz, C_6H_5), 7.59 (t, 2H, *H-9,9'*, $^3J_{H\text{-}H}$ = 7.4 Hz, C_6H_5), 7.71 (ddd, 1H, *H-4*, $^3J_{H\text{-}H}$ = 7.5 Hz, $^4J_{H\text{-}H}$ = 1.2 Hz, C_6H_4), 7.95 (dd, 1H, *H-3*, $^3J_{H\text{-}H}$ = 7.6 Hz, $^4J_{H\text{-}H}$ = 1.3 Hz, C_6H_4), 8.14 (ddd, 1H, *H-5*, $^3J_{H\text{-}H}$ = 7.5 Hz, $^4J_{H\text{-}H}$ = 1.3 Hz, C_6H_4), 10.04 (dd, 1H, *H-6*, $^3J_{H\text{-}H}$ = 7.7 Hz, $^4J_{H\text{-}H}$ = 1.3 Hz, C_6H_4). $^{13}C\{^1H\}$ NMR (125.81 MHz, $CDCl_3$): δ 128.27 (s, *C-8,8'*), 129.47 (s, *C-10*), 129.92 (s, *C-4*), 130.55 (s, *C-9,9'*), 132.95 (s, *C-3*), 135.37 (s, *C-5*), 140.70 (s, *C-6*), 142.13 (s, *C-7*), 147.84 (s, *C-2*), *C-1* could not be detected.

*Synthesis of (2-PhC$_6$H$_4$)BiI$_2$ (**8**)*

Solid KI (0.154 g, 0.92 mmol) was added to a solution of (2-PhC_6H_4)$BiBr_2$ (**8**) (0.202 g, 0.38 mmol) in EtOH (20 mL). The color of the solution turned immediately orange and the reaction mixture was stirred for three days at ambient temperature. After removal of solvent under vacuo, the orange powder was extracted with toluene (3 x 5 mL), the solution filtered and the solvent was removed under vacuo to give an orange powder. Single crystals suitable for X-ray analysis were grown from a CH_2Cl_2 solution at ambient temperature. Yield: 0.095 g, (40 %). M.p. = 161-162 °C, dec. Elemental analysis calcd. (%) for $C_{12}H_9BiI_2$ (615.99 g·mol^{-1}): C, 23.40; H, 1.47. Found: C, 22.93; H,1.34. ATR FTIR (cm^{-1}): 3054 (m), 2359 (w), 2339 (w), 2326 (w), 1969 (w), 1947 (w), 1902 (w), 1885 (w), 1860 (w), 1831 (w), 1815 (w), 1764 (w), 1731 (w), 1702 (w), 1656 (w), 1627 (w), 1594 (m), 1573 (m), 1548 (m), 1527 (w), 1490 (m), 1452 (s),

DOI: 10.1039/C9CP06924K

1440 (s), 1423 (s), 1411 (s), 1390 (m), 1336 (w), 1315 (m), 1311 (m), 1286 (m), 1273 (m), 1240 (m), 1178 (s), 1161 (s), 1070 (s), 1057 (s), 1032 (m), 1015 (m), 1003 (s), 983 (s), 970 (s), 949 (s), 920 (s), 874 (m), 849 (s), 774 (s), 745 (vs), 716 (s), 704 (vs), 666 (w), 642 (m), 613 (s), 550 (s), 517 (s), 425 (s), 408 (m). ^{1}H NMR (500.30 MHz, CDCl$_3$): δ 7.41 (m, 2H, *H-8,8'*, C$_6$*H*$_5$), 7.50 (t, 1H, *H-10,* $^3J_{H\text{-}H}$ = 7.4 Hz, C$_6$*H*$_5$), 7.57 (t, 2H, *H-9,9'*, $^3J_{H\text{-}H}$ = 7.3 Hz, C$_6$*H*$_5$), 7.70 (ddd, 1H, *H-4*, $^3J_{H\text{-}H}$ = 7.4 Hz, $^4J_{H\text{-}H}$ = 1.2 Hz, C$_6$*H*$_4$), 7.78 (dd, 1H, *H-3*, $^3J_{H\text{-}H}$ = 7.6 Hz, $^4J_{H\text{-}H}$ = 1.4 Hz, C$_6$*H*$_4$), 7.93 (ddd, 1H, *H-5*, $^3J_{H\text{-}H}$ = 7.5 Hz, $^4J_{H\text{-}H}$ = 1.4 Hz, C$_6$*H*$_4$), 10.42 (d, 1H, *H-6*, $^3J_{H\text{-}H}$ = 7.7 Hz, C$_6$*H*$_4$). ^{13}C{^{1}H} NMR (125.81 MHz, CDCl$_3$): δ 127.68 (s, *C-8,8'*), 129.39 (s, *C-4*), 129.70 (s, *C-10*), 130.23 (s, *C-9,9'*), 131.53 (s, *C-3*), 135.86 (s, *C-5*), 142.79 (s, *C-7*), 146.35 (s, *C-6*), 147.29 (s, *C-2*), *C-1* could not be detected.

*Synthesis of (2-PhC$_6$H$_4$)$_3$Sb (**9**)*

A solution of ^{n}BuLi in n-hexane (2.33 mL, 2.5 M, 5.83 mmol) was added dropwise, at −78 °C, to a stirred solution of 2-bromobiphenyl (1.130 g, 4.85 mmol) in anhydrous Et$_2$O (35 mL). The reaction mixture was stirred for 2 h at −78 °C. After that the organolithium compound was added dropwise to a solution of SbCl$_3$ (1.106 g, 4.85 mmol) in Et$_2$O (50 mL), the reaction mixture was kept at −78 °C for 2 h and then stirred overnight at ambient temperature. The solvent was evacuated in vacuo and the creamy precipitate was extracted with toluene (3 x 10 mL), the solution filtrated and after removal of the solvent in vacuo, a colorless powder was isolated. Single crystals suitable for X-ray analysis were grown from a CH$_2$Cl$_2$ solution. Yield: 0.228 g (24 %). M.p. = 214-215 °C. Elemental analysis calcd. (%) for C$_{36}$H$_{27}$Sb (581.36 g·mol-1): C, 74.38; H, 4.68. Found: C, 73.89; H, 4.62. ATR FTIR (cm^{-1}): 3054 (m), 3033 (m), 2364 (w), 2322 (w), 1927 (w), 1822 (w), 1752 (w), 1598 (w), 1577 (m), 1559 (w), 1494 (m), 1456 (s), 1440 (s), 1419 (s), 1382 (w), 1332 (w), 1282 (w), 1244 (m), 1178 (m), 1161 (m), 1111 (m), 1074 (m), 1032 (w), 1023 (w), 1008 (s), 995 (w), 983 (w), 966 (w), 949 (m), 907 (m), 874 (w), 841 (m), 770 (s), 749 (vs), 730 (s), 697 (vs), 671 (m), 649 (m), 616 (s), 571 (w), 546 (s), 533 (s), 488 (w), 452 (s), 446 (s), 440 (s), 413 (w), 401 (w). ^{1}H NMR (500.30 MHz, CDCl$_3$): δ 6.97–7.02 (m, 6H, *H-8,8'*, C$_6$H$_5$), 7.13–7.21 (m, 9H, *H-9,9'*, *H-10*, C$_6$*H*$_5$), 7.22–7.29 (m, 6H, H-

3, *H-4*, C_6H_4), 7.35–7.38 (m, 6H, *H-5* and *H-6*, C_6H_4). $^{13}C\{^1H\}$ NMR (125.81 MHz, $CDCl_3$): δ 127.19 (s, *C-10*), 127.65 (s, *C-4*), 127.98 (s, *C-9,9'*), 128.43 (s, *C-3*), 129.21 (s, *C-5*), 129.30 (s, *C-8,8'*), 137.45 (s, *C-6*), 140.70 (s, *C-1*), 143.89 (s, *C-7*), 149.70 (s, *C-2*).

Acknowledgements

We gratefully acknowledge financial support from the DFG SPP1807 "*Control of London Dispersion Interactions in Molecular Chemistry*". We thank Prof. S. Spange for access to the IR instrument. We are grateful to Anja Veit and Lutz Mertens for measuring the IR spectra and PXRD, respectively. We also thank Ute Stöß and Janine Freytag for performing the CHN analyses. We thank Sebastian Scharf und Sebastian Notz for measuring the temperature dependent NMR spectra. M. Korb thanks the Fonds der Chemischen Industrie for a Ph.D. Chemiefonds fellowship. Ana Toma is grateful for financial support from the DAAD within the frame of the Eastern Europe Partnership program. Cristian Silvestru is grateful for financial support by TU Chemnitz of a short term scientific guest exchange. Anca Silvestru is thanked for ongoing fruitful cooperation in the field of organometallic synthesis.

References:

1. C. Silvestru, H. J. Breunig and H. Althaus, *Chem. Rev.*, 1999, **99**, 3277-3328.
2. H. Schmidbaur and A. Schier, *Organometallics*, 2008, **27**, 2361-2395.
3. V. M. Cangelosi, M. A. Pitt, W. J. Vickaryous, C. A. Allen, L. N. Zakharov and D. W. Johnson, *Cryst. Growth Des.*, 2010, **10**, 3531-3536.
4. J. Zukerman-Schpector and E. R. T. Tiekink, in *The Importance of Pi-Interactions in Crystal Engineering*, John Wiley & Sons, Ltd, 2012, pp. 275-299.
5. M. M. Watt, M. S. Collins and D. W. Johnson, *Acc. Chem. Res.*, 2013, **46**, 955-966.
6. I. Caracelli, I. Haiduc, J. Zukerman-Schpector and E. R. T. Tiekink, *Coord. Chem. Rev.*, 2013, **257**, 2863-2879.
7. I. Caracelli, J. Zukerman-Schpector, I. Haiduc and E. R. T. Tiekink, *CrystEngComm*, 2016, **18**, 6960-6978.
8. E. R. T. Tiekink, *Coord. Chem. Rev.*, 2017, **345**, 209-228.
9. D. J. Liptrot and P. P. Power, *Nature Rev. Chem.*, 2017, **1**, 0004.
10. W. B. Schneider, G. Bistoni, M. Sparta, M. Saitow, C. Riplinger, A. A. Auer and F. Neese, *J. Chem. Theory Comput.*, 2016, **12**, 4778-4792.
11. S. Grimme, A. Hansen, J. G. Brandenburg and C. Bannwarth, *Chem. Rev.*, 2016, **116**, 5105-5154.
12. G. Bistoni, A. A. Auer and F. Neese, *Chem. Eur. J.*, 2017, **23**, 865-873.
13. R. Lo, P. Švec, Z. Růžičková, A. Růžička and P. Hobza, *Chem. Commun.*, 2016, **52**, 3500-3503.
14. A. Bauzá, D. Quiñonero, P. M. Deyà and A. Frontera, *CrystEngComm*, 2013, **15**, 3137-3144.

15. A. Bauzá, D. Quiñonero, P. M. Deyà and A. Frontera, *Phys. Chem. Chem. Phys.*, 2012, **14**, 14061-14066.
16. A. A. Auer, D. Mansfeld, C. Nolde, W. Schneider, M. Schürmann and M. Mehring, *Organometallics*, 2009, **28**, 5405-5411.
17. D. Mansfeld, M. Mehring and M. Schürmann, *Z. Anorg. Allg. Chem.*, 2004, **630**, 1795-1797.
18. A. M. Preda, W. B. Schneider, M. Rainer, T. Rüffer, D. Schaarschmidt, H. Lang and M. Mehring, *Dalton Trans.*, 2017, **46**, 8269-8278.
19. A. M. Toma, A. Pop, A. Silvestru, T. Rüffer, H. Lang and M. Mehring, *Dalton Trans.*, 2017, **46**, 3953-3962.
20. A. M. Preda, M. Krasowska, L. Wrobel, P. Kitschke, P. C. Andrews, J. G. MacLellan, L. Mertens, M. Korb, T. Rüffer, H. Lang, A. A. Auer and M. Mehring, *Beilstein J. Org. Chem.*, 2018, **14**, 2125-2145.
21. A. M. Preda, W. B. Schneider, D. Schaarschmidt, H. Lang, L. Mertens, A. A. Auer and M. Mehring, *Dalton Trans.*, 2017, **46**, 13492-13501.
22. L. Wrobel, T. Rüffer, M. Korb, H. Krautscheid, J. Meyer, P. C. Andrews, H. Lang and M. Mehring, *Chem. Eur. J.*, 2018, **24**, 16630-16644.
23. K. Srinivas, P. Suresh, C. N. Babu, A. Sathyanarayana and G. Prabusankar, *RSC Advances*, 2015, **5**, 15579-15590.
24. H. J. Breunig, N. Haddad, E. Lork, M. Mehring, C. Mügge, C. Nolde, C. I. Raţ and M. Schürmann, *Organometallics*, 2009, **28**, 1202-1211.
25. C. Hering-Junghans, M. Thomas, A. Villinger and A. Schulz, *Chem. Eur. J.*, 2015, **21**, 6713-6717.
26. C. Hering-Junghans, A. Schulz and A. Villinger, *Chem. Commun.*, 2015, **51**, 13834-13837.
27. C. Hering-Junghans, A. Schulz, M. Thomas and A. Villinger, *Dalton Trans.*, 2016, **45**, 6053-6059.
28. B. Twamley, C. D. Sofield, M. M. Olmstead and P. P. Power, *J. Am. Chem. Soc.*, 1999, **121**, 3357-3367.
29. J. Bresien, C. Hering-Junghans, A. Schulz, M. Thomas and A. Villinger, *Organometallics*, 2018, **37**, 2571-2580.
30. R. J. Schwamm, C. M. Fitchett and M. P. Coles, *Chem. Asian J.*, 2019, **14**, 1204-1211.
31. A. Schulz, M. Thomas and A. Villinger, *Z. Anorg. Allg. Chem.*, 2017, **643**, 1406-1414.
32. J. Bresien, A. Schulz, M. Thomas and A. Villinger, *Eur. J. Inorg. Chem.*, 2019, 1279-1287.
33. J. Fanfrlik, R. Sedlak, A. Pecina, L. Rulisek, L. Dostal, J. Moncol, A. Ruzicka and P. Hobza, *Dalton Trans.*, 2016, **45**, 462-465.
34. M. Krasowska, W. B. Schneider, M. Mehring and A. A. Auer, *Chem. Eur. J.*, 2018, **24**, 10238-10245.
35. M. Krasowska, A.-M. Fritzsche, M. Mehring and A. A. Auer, *ChemPhysChem*, 2019, **20**, 2539-2552.
36. D. E. Worrall, *J. Am. Chem. Soc.*, 1936, **58**, 1820-1821.
37. D. E. Worrall, *J. Am. Chem. Soc.*, 1940, **62**, 2514-2515.
38. D. M. Hawley and G. Ferguson, *J. Chem. Soc. A*, 1968, 2059-2063.
39. P. G. Jones, A. Blaschette, D. Henschel and A. Weitze, *Z. Kristallogr.*, 1995, **210**, 377-378.
40. T. Ogawa, T. Ikegami, T. Hikasa, N. Ono and H. Suzuki, *J. Chem. Soc. Perkin Trans. 1*, 1994, 3479-3483.
41. V. Stavila, J. H. Thurston, D. Prieto-Centurión and K. H. Whitmire, *Organometallics*, 2007, **26**, 6864-6866.
42. S. Alvarez, *Dalton Trans.*, 2013, **42**, 8617-8636.
43. W. Clegg, R. J. Errington, G. A. Fisher, D. C. R. Hockless, N. C. Norman, A. G. Orpen and S. E. Stratford, *J. Chem. Soc., Dalton Trans.*, 1992, 1967-1974.
44. W. Clegg, R. J. Errington, G. A. Fisher, R. J. Flynn and N. C. Norman, *J. Chem. Soc., Dalton Trans.*, 1993, 637-641.

45. M. Mantina, A. C. Chamberlin, R. Valero, C. J. Cramer and D. G. Truhlar, *J. Phys.Chem. A*, 2009, **113**, 5806-5812.

46. S. Grimme, *J. Chem. Theory Comput.*, 2019, **15**, 2847-2862.

47. S. Kamepalli, C. J. Carmalt, R. D. Culp, A. H. Cowley, R. A. Jones and N. C. Norman, *Inorg. Chem.*, 1996, **35**, 6179-6183.

48. L. M. Opris, A. Silvestru, C. Silvestru, H. J. Breunig and E. Lork, *Dalton Trans.*, 2003, 4367-4374.

49. A. Soran, H. J. Breunig, V. Lippolis, M. Arca and C. Silvestru, *J. Organomet. Chem.*, 2010, **695**, 850-862.

50. H. Suzuki, T. Murafuji, Y. Matano and N. Azuma, *J. Chem. Soc. Perkin Trans. 1*, 1993, 2969-2973.

51. H. Suzuki, T. Murafuji and N. Azuma, *J. Chem. Soc. Perkin Trans. 1*, 1993, 1169-1175.

52. M. Kaupp, O. L. Malkina, V. G. Malkin and P. Pyykkö, *Chem. Eur. J.*, 1998, **4**, 118-126.

53. J. Ariai and G. Saielli, *ChemPhysChem*, 2019, **20**, 108-115.

54. M. Rubio, M. Merchan and E. Orti, *Theor. Chim. Acta*, 1995, **91**, 17-29.

55. *MestReNova*, *(version 11.0.4-18998)*, Mestrelab Research S. L., Santiago de Compostela, **2017**.

56. *ChemDraw® Prime (version 17.1)*, PerkinElmer Informatics, Waltham, MA, 2018.

57. *Origin® Pro 2017*, OriginLab, Northampton, MA, 2017.

58. G. M. Sheldrick, *SHELXS-2013, Program for Crystal Structures Solution*, University of Göttingen, 2013.

59. G. M. Sheldrick, *Acta Crystallogr., Sect. A*, 2008, **64**, 112-122.

60. G. M. Sheldrick, *SHELXL-2013, Program for Crystal Structures Refinement*, University of Göttingen, 2013.

61. G. M. Sheldrick, *Acta Crystallogr., Sect. C*, 2015, **71**, 3-8.

62. K. Brandenburg and H. Putz, *Diamond – Crystal and Molecular Structure Visualization (version 4.5)*, Bonn, 2018.

63. S. Grimme, C. Bannwarth and P. Shushkov, *J. Chem. Theory Comput.*, 2017, **13**, 1989-2009.

64. C. Bannwarth, S. Ehlert and S. Grimme, *J. Chem. Theory Comput.*, 2019, **15**, 1652-1671.

65. J. P. Perdew, K. Burke and M. Ernzerhof, *Phys. Rev. Lett.*, 1996, **77**, 3865-3868.

66. J. P. Perdew, K. Burke and M. Ernzerhof, *Phys. Rev. Lett.*, 1997, **78**, 1396-1396.

67. F. Weigend and R. Ahlrichs, *Phys. Chem. Chem. Phys.*, 2005, **7**, 3297-3305.

68. F. Weigend, *Phys. Chem. Chem. Phys.*, 2006, **8**, 1057-1065.

69. B. Metz, H. Stoll and M. Dolg, *J. Chem. Phys.*, 2000, **113**, 2563-2569.

70. K. A. Peterson, D. Figgen, E. Goll, H. Stoll and M. Dolg, 2003, **119**, 11113-11123.

71. S. Grimme, J. Antony, S. Ehrlich and H. Krieg, *J. Chem. Phys.*, 2010, **132**, 154104.

72. S. Grimme, S. Ehrlich and L. Goerigk, *J. Comput. Chem.*, 2011, **32**, 1456-1465.

73. A. D. Becke and E. R. Johnson, *J. Chem. Phys.*, 2005, **123**, 154101.

74. F. Neese, A. Hansen and D. G. Liakos, *J. Chem. Phys.*, 2009, **131**, 064103.

75. F. Neese, A. Hansen, F. Wennmohs and S. Grimme, *Acc. Chem. Res.*, 2009, **42**, 641-648.

76. A. Hansen, D. G. Liakos and F. Neese, *J. Chem. Phys.*, 2011, **135**, 214102.

77. D. G. Liakos, A. Hansen and F. Neese, *J. Chem. Theory Comput.*, 2011, **7**, 76-87.

78. C. Riplinger and F. Neese, *J. Chem. Phys.*, 2013, **138**, 034106.

79. C. Riplinger, B. Sandhoefer, A. Hansen and F. Neese, *J. Chem. Phys.*, 2013, **139**, 134101.

80. C. Riplinger, P. Pinski, U. Becker, E. F. Valeev and F. Neese, *J. Chem. Phys.*, 2016, **144**, 024109.

81. T. H. Dunning, *J. Chem. Phys.*, 1989, **90**, 1007-1023.

82. K. A. Peterson, *J. Chem. Phys.*, 2003, **119**, 11099-11112.

83. K. A. Peterson and K. E. Yousaf, *J. Chem. Phys.*, 2010, **133**, 174116.

84. F. Weigend, *J. Comput. Chem.*, 2008, **29**, 167-175.

85. F. Weigend, A. Kohn and C. Hattig, *J. Chem. Phys.*, 2002, **116**, 3175-3183.

86. C. Hättig, G. Schmitz and J. Koßmann, *Phys. Chem. Chem. Phys.*, 2012, **14**, 6549-6555.

87. D. G. Liakos and F. Neese, *J. Chem. Theory Comput.*, 2015, **11**, 4054-4063.

View Article Online
DOI: 10.1039/C9CP06924K

88. D. G. Liakos, M. Sparta, M. K. Kesharwani, J. M. L. Martin and F. Neese, *J. Chem. Theory Comput.*, 2015, **11**, 1525-1539.
89. Y. Zhao and D. G. Truhlar, *J. Chem. Phys.*, 2006, **125**, 194101.
90. J. Tao, J. P. Perdew, V. N. Staroverov and G. E. Scuseria, *Phys. Rev. Lett.*, 2003, **91**, 146401.
91. F. Jensen, *J. Chem. Theory Comput.*, 2015, **11**, 132-138.
92. T. Noro, M. Sekiya and T. Koga, *Theor. Chem. Acc.*, 2013, **132**, 1363.
93. G. L. Stoychev, A. A. Auer and F. Neese, *J. Chem. Theory Comput.*, 2017, **13**, 554-562.
94. E. J. Baerends, D. E. Ellis and P. Ros, *Chem. Phys.*, 1973, **2**, 41-51.
95. J. L. Whitten, *J. Chem. Phys.*, 1973, **58**, 4496-4501.
96. B. I. Dunlap, J. W. D. Connolly and J. R. Sabin, *J. Chem. Phys.*, 1979, **71**, 3396-3402.
97. M. Feyereisen, G. Fitzgerald and A. Komornicki, *Chem. Phys. Lett.*, 1993, **208**, 359-363.
98. O. Vahtras, J. Almlöf and M. W. Feyereisen, *Chem. Phys. Lett.*, 1993, **213**, 514-518.
99. K. Eichkorn, O. Treutler, H. Öhm, M. Häser and R. Ahlrichs, *Chem. Phys. Lett.*, 1995, **240**, 283-290.
100. R. A. Kendall and H. A. Fruchtl, *Theor. Chem. Acc.*, 1997, **97**, 158-163.
101. F. Weigend and M. Haser, *Theor. Chem. Acc.*, 1997, **97**, 331-340.
102. F. Weigend, M. Häser, H. Patzelt and R. Ahlrichs, *Chem. Phys. Lett.*, 1998, **294**, 143-152.